Neuronal Activity in the Globus Pallidus in Chorea Caused by Striatal Lacunar Infarction

Takao Hashimoto, MD, PhD,[1]
Hiroshi Morita, MD, PhD,[1] Tsuyoshi Tada, MD, PhD,[2]
Tetsuhiro Maruyama, MD, PhD,[3]
Yuzo Yamada, MD, PhD,[4]
and Shu-ichi Ikeda, MD, PhD[1]

Pallidotomy was performed in a patient with hemichorea caused by lacunar infarction in the striatum. Chorea in the lower limb was reduced after a neurosurgical lesion in the medial portion of the sensorimotor territory of the internal segment of the globus pallidus, and chorea in the upper limb disappeared after an additional lesion in the lateral portion of that same area. Intraoperative neuronal recording revealed that mean firing rates were low, and that firing was irregular in the globus pallidus compared with off-state parkinsonian patients. These results suggest that chorea with striatal infarction is driven by phasic neuronal activity with a low firing rate in the globus pallidus and that the neural pathway of chorea has a functional somatotopical organization in the globus pallidus.

Ann Neurol 2001;50:528–531

Decreased activity of the basal ganglia output nuclei has been proposed as a central mechanism underlying hyperkinetic disorders.[1,2] Decreased firing rates have been demonstrated by intraoperative neuronal recording in patients with hemiballismus caused by subthalamic lesions[3–5] and in those with apomorphine-induced dyskinesia,[6] while neuronal changes of the pallidum in chorea caused by vascular striatal lesions[7,8] have not been elucidated. We report on changes in the firing pattern in the pallidal neurons and the effects of pallidotomy in a patient with chorea caused by ischemic striatal lesions.

Case Report

A 75-year-old hypertensive woman, with a history of transient right hemiparesis 3 years before, acutely developed involuntary movements of the right upper and lower limbs. She had no neuroleptic exposure, rheumatic fever, or family history of chorea. Examination revealed choreiform movements in the right upper and lower limbs without paresis. She had no mental impairment. Laboratory tests revealed no hematologic abnormalities, including negative antinuclear antibody. Magnetic resonance images (MRIs) taken 2 months after onset demonstrated multiple small, hyperintense foci on T2-weighted images in the bilateral putamen, left caudate, and left globus pallidus (lacunar infarcts); some of these foci were hypointense on T1-weighted images, suggesting enlarged Virchow-Robin spaces *(état criblé)*.[9] No lesion was shown in the subthalamic nuclear areas (Fig 1). These findings were confirmed by an MRI taken 13 months after the first one. The patient was treated with 3mg haloperidol daily, and the choreiform movements were ameliorated. Three months later, parkinsonian signs, consisting of severe bradykinesia, rigidity, and dysphagia, appeared and led to reduction in the haloperidol dose, resulting in exacerbation of the choreiform movements. At the time of surgery, performed 15 months after onset, she took no neuroleptic medication and showed choreiform movements severely in the right lower limb and mildly in the right upper limb, as well as mild lingual dyskinesia. Electromyograms (EMGs) recorded from the right extremities revealed repetitive reciprocal discharges in the pretibial and gastrocnemius-soleus muscles with a 3- to 5-second interval and repetitive discharges in the wrist flexor muscles intermittently synchronized to the leg EMGs.

To improve the medically intractable involuntary movements, left pallidotomy was performed with microelectrode guidance. No sedation was used in surgery, and all medications were withheld overnight and during surgery. Glass-coated elgiloy microelectrodes with an impedance of 0.4MΩ at 1,000Hz were used for single-cell recording. Recording tracks were made in the parasagittal plane, proceeding from anterodorsal to posteroventral at an angle of 45 degrees from the vertical line. The lateral distance of the electrode tip to the cerebral midline was measured by intraoperative computed tomography. After electrophysiological mapping, the coagulation electrode (diameter 1.2mm, exposed tip length 3mm) was advanced for lesioning in two tracks, the first track at lateral 19mm and the second track at lateral 21mm.

Ten- to 30-second samples of spontaneous single-cell activity from the external globus pallidus (GPe) and the internal globus pallidus (GPi) were recorded during mapping and stored on digital tape. Neuronal signals were digitized at 50kHz, action potentials discriminated, interspike interval data stored, and firing rates calculated. Cross-correlation analysis was carried out to determine whether the neuronal signals and EMG signals correlated. The level of chance correlation was calculated using the control spike trains. Eight control spike trains were made by randomizing the order of the interspike intervals of the original neuronal signal of the patient, and significant levels were determined by means ± 2 standard deviations (SD) of the maximal or minimal correlation coefficients. Student's *t* test (two-tailed) was used to determine the level of statistical significance when comparing mean firing rates in the present patient with those in off-state parkinsonian patients.

From the [1]Third Department of Medicine and [2]Department of Neurosurgery, Shinshu University School of Medicine, Matsumoto; and Departments of [3]Neurology and [4]Neurosurgery, Kakeyu Rehabilitation Center and Clinic, Maruko, Japan.

Received Feb 6, 2001, and in revised form Jun 6. Accepted for publication Jun 23, 2001.

Published online Sep 3, 2001; DOI: 10.1002/ana.1229

Address correspondence to Dr Hashimoto, Third Department of Medicine, Shinshu University School of Medicine, Asahi 3-1-1, Matsumoto 390-8621, Japan. E-mail: takahhh@hsp.md.shinshu-u.ac.jp

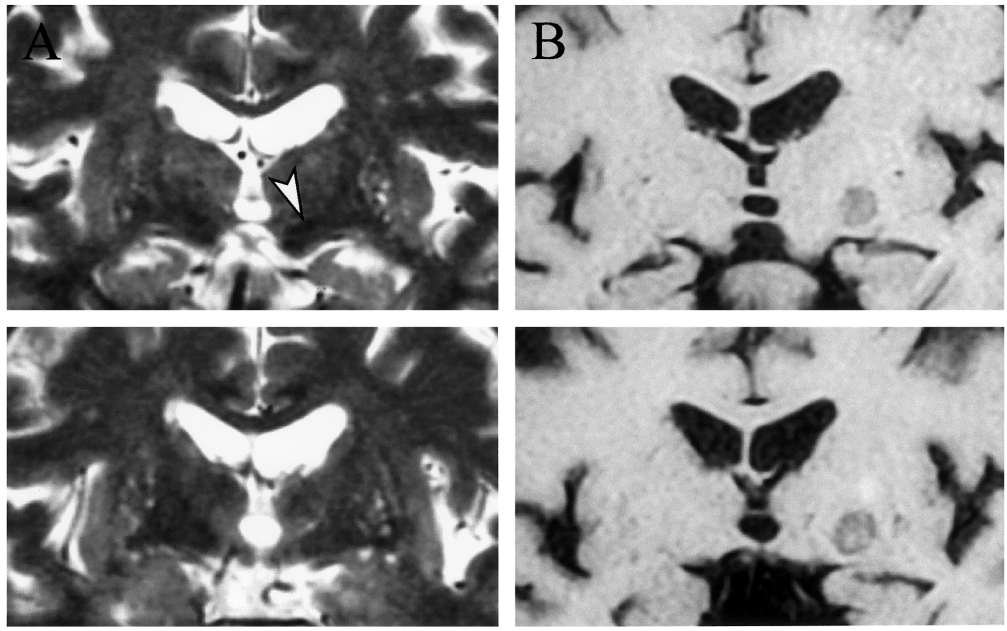

Fig 1. (A) T2-weighted frontal magnetic resonance images (slices 10 and 15mm posterior to anterior commissure) 2 months after onset, showing multiple lacunar infarcts and état criblé *in the bilateral striata, without involvement in the left subthalamic area* (arrowhead). *(B) T1-weighted images (same slice location as in A) 10 days after surgery, following pallidotomy, showing the surgical lesion with surrounding edema.*

Results

The recording sites and coagulation sites are illustrated in Figure 2A. The activity of 11 cells was sampled from the GPe and GPi along the third track at lateral 18.0mm, and along the fifth and sixth tracks at lateral 19.0mm. The frequency of 4 GPe cells (mean ± SD 49.6 ± 12.4Hz) was not significantly different ($p < 0.2$) from that in parkinsonian patients without dyskinesia (56 cells from 13 patients; 59.6 ± 19.8Hz). The frequency of 7 GPi cells (56.7 ± 21.1Hz) was significantly lower ($p < 0.005$) than that in patients without dyskinesia (85 cells from 16 patients; 89.5 ± 25.7Hz). The activity of one of the 11 neurons in the present patient correlated with chorea EMG activity from the wrist flexor muscles, pretibial muscles, and gastrocnemius-soleus muscles (Fig 3). The regularity in the cross-correlation functions with approximately 4.5 seconds duration between the neuronal signals and EMGs from the lower limb reflects the periodicity of the chorea EMG discharges. This and the other neurons could not be recorded long enough to test for kinesthetic responses.

After coagulations along the first coagulation track at lateral 19mm, leg choreiform movements were remarkably reduced without change in arm choreiform movements (see Fig 2C). After coagulations along the second coagulation track at lateral 21mm, arm and leg choreiform movements almost disappeared (see Fig 2D). Choreiform movements contralateral to the surgery were completely abolished after surgery and have not returned over the follow-up period, which is now longer than 2 years, but mild lingual dyskinesia persisted.

Discussion

Acute-onset hemichorea in our patient suggests a vascular pathogenesis, and rhythmic choreiform movements demonstrated by EMG are also characteristic of vascular chorea.[10] Repeated MRI studies depicted lacunar infarcts in the striatum without apparent involvement of the subthalamic nucleus. From these findings, we conclude that the hemichorea in this patient was most probably due to striatal lacunar infarction, which is known to be one of the causative lesions of hemichorea outside the subthalamic nucleus.[7,8] Mild lingual dyskinesia may have been tardive dyskinesia following haloperidol administration.

In the case of hemiballismus, reduced activity in both the GPi and GPe has been demonstrated in monkeys[11,12] and humans,[3–5] and destruction of the subthalamus-GPe and subthalamus-GPi excitatory pathways by subthalamic lesions is assumed to cause these changes. Decreased activity in the GPi with overactivity in the GPe has been observed in apomorphine-induced dyskinesia in parkinsonian laboratory animals[13] and humans[6]; overactivity of the striatum-GPi inhibitory pathway by D1 receptor stimulation and reduced activity of the striatum-GPe inhibitory pathway by D2 receptor stimulation may cause these changes.[14] Firing rates in the GPi were significantly lower than

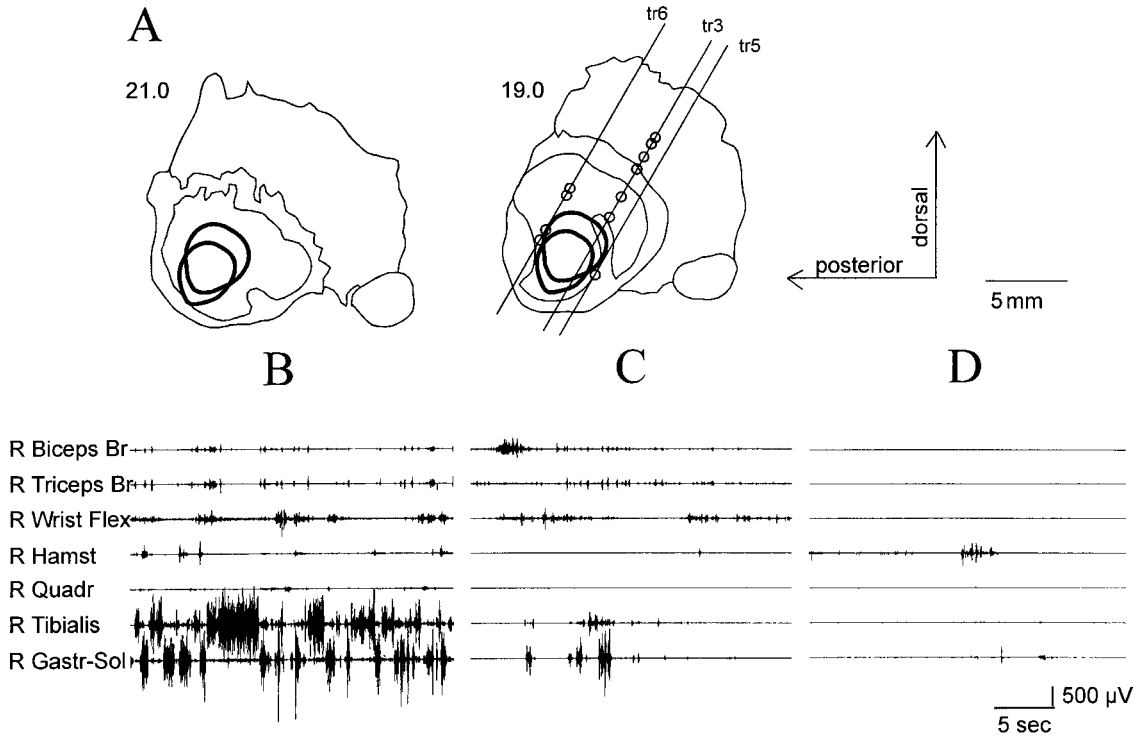

Fig 2. (A) Reconstruction of the trajectories (tracks 3, 5, *and* 6) *through the external and internal segments of the globus pallidus* (GPi) *and the recording sites* (open circles) *illustrated on the sagittal brain maps (nearest planes from Schaltenbrand and Bailey atlas[19]).* Track 3 *at 18mm to midline and* tracks 5 *and* 6 *at 19mm are drawn in the same plane. The lateral location was measured by intraoperative computed tomography. Electromyograms (EMGs) from the right upper and lower limbs recorded during pallidotomy before coagulation (B), after coagulation along the first coagulation track at lateral 19mm (C), and after coagulations along the second coagulation track at lateral 21mm (D). Chorea EMGs from the lower limb were markedly reduced after coagulation in the medial portion, and those from the upper limb disappeared after coagulation in the lateral portion.*

those in off-state Parkinson's disease in the present patient, suggesting that decreased firing rate in the GPi is the underlying abnormality in chorea caused by ischemic striatal lesions, as well as in other choreic disorders. However, firing rates in the GPe were not different from those in Parkinson's disease. Since the number of GPe neurons studied is too small to be conclusive, the contribution of the direct and indirect pathways to GPi underactivity remains obscure.

The development of choreiform movements depends on choreogenic neuronal activity in the brain. An irregular, or bursting and pausing, firing pattern in the GPi has commonly been observed in hemiballismus patients,[3–5] and correlation between neuronal activity and EMGs has been observed in some GPi neurons of a patient with hemiballismus.[5] The firing pattern in the GPi was also irregular and phasic in the present patient compared with that in Parkinson's disease, and one GPi neuron showed a time correlation to the chorea EMGs recorded from the upper and lower limbs. While it may indicate choreogenic neuronal drive in the GPi, this correlation could result from feedback response to peripheral sensory stimuli associated with choreiform movements. The synchronous pauses following the high-frequency firing in the GPi may cause phasic cortical disinhibition, resulting in ballismus. It has been noted before that improvement in choreiform movements with pallidotomy procedures is paradoxical because a reduction of basal ganglia output by such lesions could be expected to further disinhibit the cortex. Appreciation of this paradox has led to the proposal that altered pallidal firing patterns may be of critical importance in the development of chorea.

Intraoperative EMG analysis and continued neurological examination demonstrated that lesioning in the medial portion of the GPi sensorimotor territory improved the leg chorea, and that lesioning in the lateral portion improved the arm chorea in this patient. Physiologic and anatomical studies in normal monkeys have demonstrated the existence of a somatotopical organization[15,16] and subchannels with different cortical origins in the basal ganglia.[17] Similar body representations have been observed in parkinsonian patients, eg, leg representation located medial and dorsal to arm and face representations,[18] and coagulation effects on parkinsonian signs occasionally follow the representations.[18] The results in our patient suggest that the neural pathways potentially related to the development of chorea have a somatotopi-

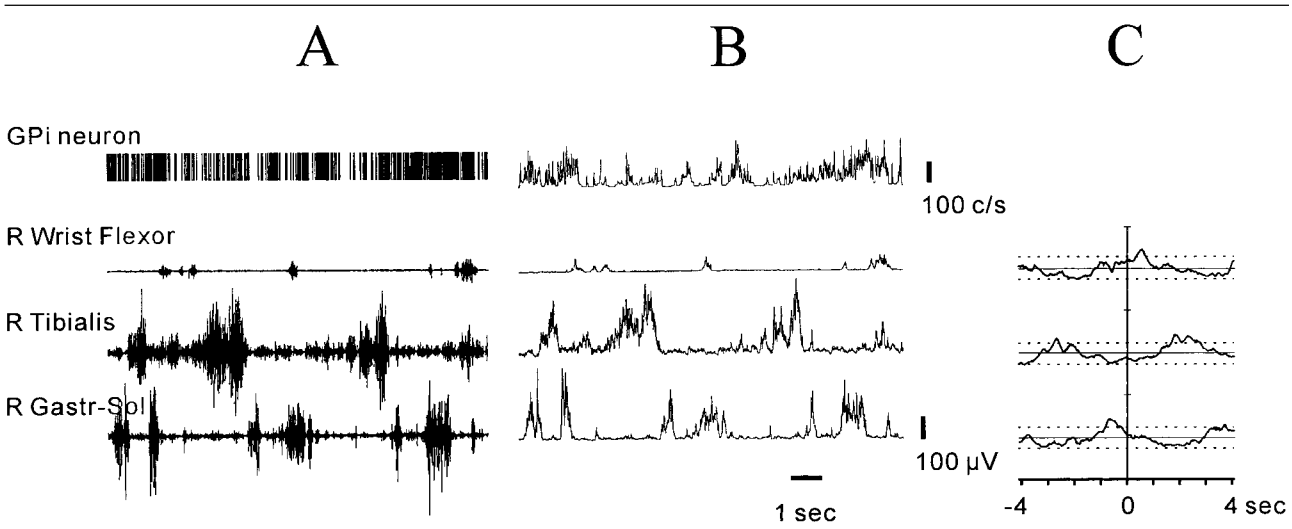

Fig 3. (A) Spike train of a neuron in the internal segment of the globus pallidus and EMGs simultaneously recorded from the right upper and lower limbs. Signals were sampled at 1kHz. Chorea EMGs from the pretibial and gastrocnemius-soleus muscles appeared reciprocally. (B) Instantaneous firing rate of a neuron and rectified EMGs converted from the signals in A and smoothed with 20-point averaging. (C) Cross-correlation functions between neuronal firing and EMGs calculated from the data in B. Dashed lines indicate maximal levels of chance correlation. Small vertical bars show the range from −1 to +1. Maximal correlation coefficients were 0.45 at +576msec between neuronal signals and EMG signals from the wrist flexor muscles (muscle activity preceding neuronal activity), 0.43 at +1,824msec between neurons and pretibial muscles, and 0.44 at −672msec between neurons and gastrocnemius-soleus muscles.

cal organization in the GPi that corresponds to the body representations demonstrated by neuronal responses to somatosensory stimuli or active movements.

We thank Dr T. Wichmann for critical reading of the manuscript.

References

1. DeLong MR. Primate models of movement disorders of basal ganglia origin. Trends Neurol 1990;13:281–285.
2. Crossman AR. Primate models of dyskinesia: the experimental approach to the study of basal ganglia–related involuntary movement disorders. Neuroscience 1987;21:1–40.
3. Suarez JI, Metman LV, Reich SG, et al. Pallidotomy for hamiballismus: efficacy and characteristics of neuronal activity. Ann Neurol 1997;42:807–811.
4. Lenz FA, Suarez JI, Verhagen Metman L, et al. Pallidal activity during dystonia: somatosensory reorganization and changes with severity. J Neurol Neurosurg Psychiatry 1998;65: 767–770.
5. Vitek JL, Chockkan V, Zhang JY, et al. Neuronal activity in the basal ganglia in patients with generalized dystonia and hemiballismus. Ann Neurol 1999;46:22–35.
6. Lozano AM, Lang AE, Levy R, et al. Neuronal recordings in Parkinson's disease patients with dyskinesias induced by apomorphine. Ann Neurol 2000;47(Suppl 1):S141–S146.
7. Schwarz GA, Barrows LJ. Hemiballism without involvement of Luy's body. Arch Neurol 1960;2:420–434.
8. Kase CS, Maulsby GO, de Juan E, Mohr JP. Hemichorea-hemiballism and lacunar infarction in the basal ganglia. Neurology 1981;31:452–455.
9. Taveras JM. Neuroradiology. Baltimore: Williams & Wilkins, 1996.
10. Hashimoto T, Yanagisawa N. A comparison of the regularity of involuntary muscle contractions in vascular chorea with that in Huntington's chorea, hemiballism and parkinsonian tremor. J Neurol Sci 1994;125:87–94.
11. Michell IJ, Sambrook MA, Crossman AR. Subcortical changes in the regional uptake of [^{3}H]-2-deoxyglucose in the brain of the monkey during experimental choreiform dyskinesia elicited by injection of a γ-aminobutyric acid antagonist into the subthalamic nucleus. Brain 1985;108:405–422.
12. Hamada I, DeLong MR. Excitotoxic acid lesions of the primate subthalamic nucleus result in reduced pallidal neuronal activity during active holding. J Neurophysiol 1992;68:1859–1866.
13. Filion M, Tremblay L, Bédard PJ. Effects of dopamine agonists on the spontaneous activity of globus pallidus neurons in monkeys with MPTP-induced parkinsonism. Brain Res 1991;547: 152–161.
14. Gerfen CR, Engber TM, Mahan LC, et al. D1 and D2 dopamine receptor–regulated gene expression of striatoni-gral and striatopallidal neurons. Science 1990;250:1429–1432.
15. DeLong MR, Crutcher MD, Georgopoulos AP. Primate globus pallidus and subthalamic nucleus: functional organization. J Neurophysiol 1985;53:530–543.
16. Alexander GE, DeLong MR. Microstimulation of the primate neostriatum. II. Somatotopic organization of striatal microexcitable zone and their relation to neuronal response properties. J Neurophysiol 1985;53:1401–1416.
17. Hoover JE, Strick PL. Multiple output channels in the basal ganglia. Science 1993;259:819–821.
18. Vitek LJ, Bakay RAE, Hashimoto T, et al. Microelectrode-guided pallidotomy: technical approach and its application in medically intractable Parkinson's disease. J Neurosurg 1998;88:1027–1043.
19. Shaltenbrand G, Bailey P. Introduction to stereotaxis with an atlas of the human brain. Stuttgart: Thieme, 1959.

Myelinopathia Centralis Diffusa (Vanishing White Matter Disease): Evidence of Apoptotic Oligodendrocyte Degeneration in Early Lesion Development

Wolfgang Brück, MD,[1,3] Jochen Herms, MD,[1] Knut Brockmann, MD,[2] Walter Schulz-Schaeffer, MD,[1] and Folker Hanefeld, MD[2]

We describe histopathological changes in a 2-year-old boy who died from myelinopathia centralis diffusa. Despite extensive white matter destruction, surprisingly high numbers of oligodendrocytes expressing proteolipid protein mRNA were detected. In an active demyelinating lesion in the brainstem, oligodendrocytes showed typical signs of apoptosis. We suggest that death of mature oligodendrocytes is the critical event in the disease.

Ann Neurol 2001;50:532–536

Leukodystrophies in childhood form a large group of disorders that are mostly inherited, and are associated with an enzyme defect. However, a large group remains unclassified. During the past few years, a new type of leukoencephalopathy, termed myelinopathia centralis diffusa,[1] vanishing white matter disease,[2] or childhood ataxia with diffuse central hypomyelination,[3] has been identified.[4] The hallmark of this disease is a clinically rapid progressive syndrome with ataxia and spasticity, leading to severe impairment and death within a few years after onset.[1] Magnetic resonance imaging (MRI) shows diffuse signal hypointensity in the white matter resembling the intensity of cerebrospinal fluid (CSF).[1,2] Magnetic resonance spectroscopy reveals absence of almost all metabolites except glucose and lactate in the lesions.[1,2]

The few pathological descriptions of this leukoencephalopathy include the following features: cavitation and vacuolation of the cerebral hemispheres with myelin and axon loss, macrophage infiltration, and reactive gliosis.[5,6] The subcortical white matter (U-fibers), internal capsule, and corpus callosum are largely preserved.[2–4,7] Several studies have noted increased numbers of oligodendrocytes.[3,6,7] The present report describes detailed findings of oligodendrocyte pathology in myelinopathia centralis diffusa.

From the Departments of [1]Neuropathology and [2]Neuropediatrics, University of Göttingen, Göttingen; and [3]Department of Neuropathology, Charité, Humboldt-University, Berlin, Germany.

Received Apr 2, 2001, and in revised form Jun 20. Accepted for publication Jun 23, 2001.

Published online Aug 24, 2001; DOI: 10.1002/ana.1227

Address correspondence to Dr Brück, Institut für Neuropathologie, Charité, Campus Virchow-Klinikum, Augustenburger Platz 1, D-13353 Berlin, Germany. E-mail: wolfgang.brueck@charite.de

Case Report

The boy was the first and only child of unrelated parents. He was born prematurely at 35 weeks of gestation by cesarean section. His birth weight (1,990g) and head circumference (29.5cm) were normal according to the gestational age. The Apgar score was 8/9/10. No abnormalities were obvious during the first months of life, except for some degree of muscular hypotonia. His motor development was mildly delayed; he was sitting at 10 months and walking with support at 16 months. At the age of 11 months, an episode of fever and vomiting occurred. Eight months later, another attack of gastroenteritis and vomiting occurred, this time accompanied by ataxia and tremor. Again, he recovered. Two months later, he developed a fever plus myoclonic jerks. He became severely ill and apathic, and died from pneumonia. During his short illness, his reflexes were always preserved and brisk. There were some swallowing difficulties, but otherwise no abnormal cranial nerve findings could be obtained. In particular, his fundi were normal and he reacted normally to sound.

Intensive laboratory investigations excluded metabolic disorders of any of the known white matter diseases, such as Krabbe's disease, metachromatic leukodystrophy, Canavan's disease, or any infectious disorder. The CSF showed no signs of inflammation or infection; toxicological screening was negative. MRI revealed widespread leukoencephalopathy. Magnetic resonance spectroscopy showed a decrease of all metabolites and an increase of glucose and lactate in the white matter, as seen during the evolution of myelinopathia centralis diffusa.[1]

The family history of this boy is remarkable. More than 25 years previously, 2 siblings (brother and sister) from the father's line died at about the same age, following a similar clinical course. In 1 male case, a postmortem examination was performed and the diagnosis of leukodystrophy was made. Brain sections of this patient were made available (courtesy of Dr Peiffer, Tübingen, Germany).

Neuropathological Techniques

Paraffin sections were stained with hematoxylin and eosin, Luxol fast blue (LFB), periodic acid–Schiff, and Bielschowsky's silver impregnation.

Immunocytochemistry, In Situ Hybridization, and In Situ Tailing

Immunocytochemistry was performed with an avidin–biotin complex or an alkaline phosphatase/antialkaline phosphatase technique. The following primary antibodies were used: anti-myelin basic protein (MBP; Boehringer-Mannheim, Mannheim, Germany), anti-2′,3′-cyclic nucleotide 3′-phosphodiesterase (CNP; Biotrend, Köln, Germany), anti-

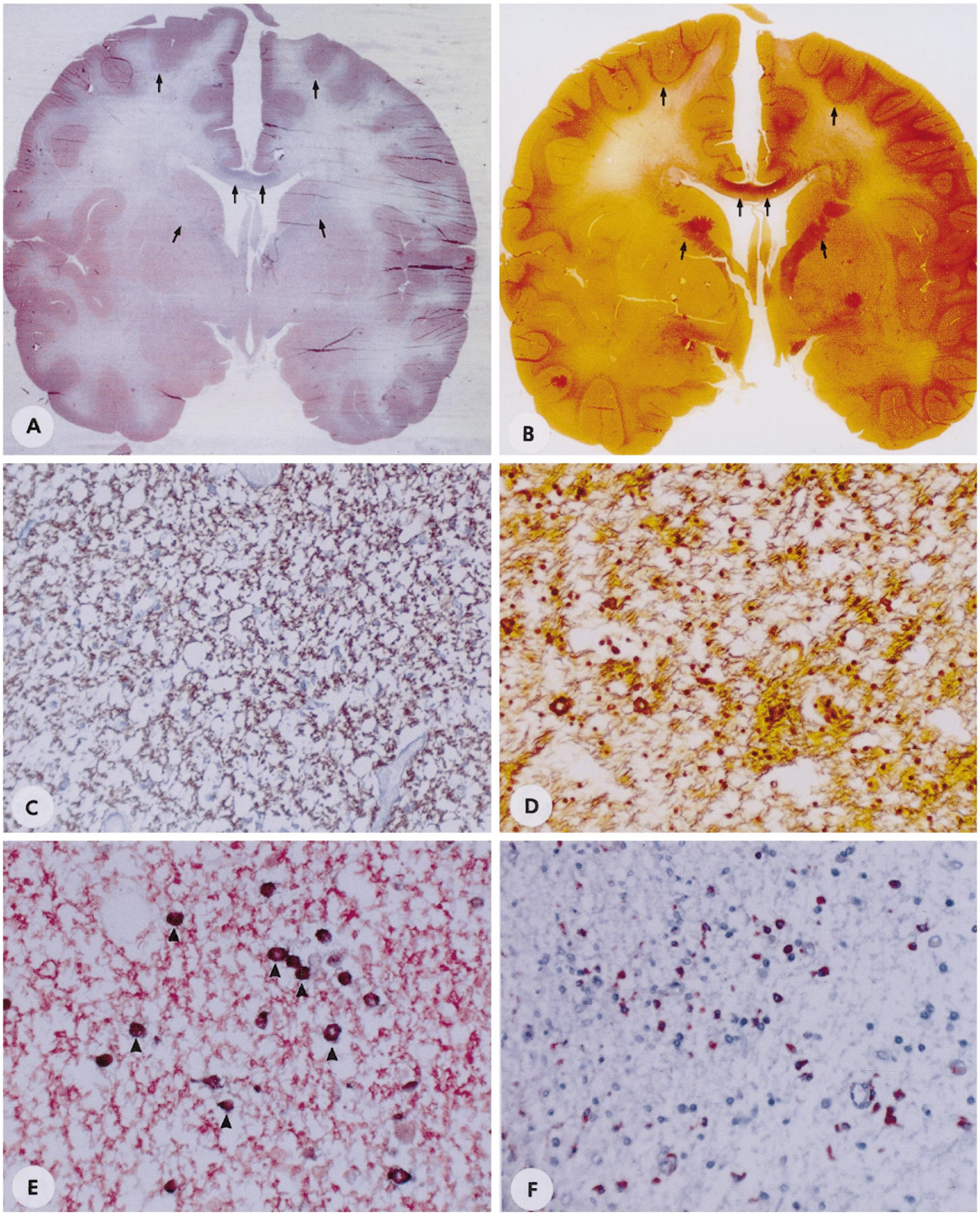

Fig 1. Pathology of cerebral white matter. (A, B) Double hemispheric sections stained for myelin with Luxol fast blue and periodic acid–Schiff (A) and Bielschowsky's silver impregnation for axons (B). (A) There is extensive myelin loss with sparing of the U-fibers, corpus callosum, and internal capsule (arrows). *(B) Axons are also rarified with similar loss and preservation* (arrows) *as myelin. (C) Higher magnification of cerebral white matter, showing thin myelin sheaths (immunocytochemistry for myelin basic protein). (D) Bielschowsky's silver impregnation reveals axon loss. (E) Oligodendrocytes* (arrowheads) *are present (in situ hybridization for proteolipid protein mRNA in black, immunocytochemistry for proteolipid protein in red). (F) Macrophages infiltrate cerebral white matter (immunocytochemistry for Ki-M1P). (C, D, and I) Magnification ×20; (E) ×40.*

Table. Numbers of Oligodendrocytes and Macrophages/Microglia per Square Millimeter in Different Brain Areas

	NAWM	Active demyelinating lesion (pons)	Inactive lesions (cerebral hemispheres)
PLP mRNA	830.0 ± 239.0	53.3 ± 61.8	300 ± 162
MOG	322.0 ± 78.0	25.0 ± 43.0	194 ± 116
Apoptotic oligodendrocytes	44.4 ± 59.8	90.0 ± 53.8	0
Macrophages/microglia	336.0 ± 107.0	808.0 ± 218.0	410 ± 160
Relative axon density (% of NAWM)	100.0	80.0 ± 9.0	30 ± 15

PLP = proteolipid protein; MOG = myelin oligodendrocyte glycoprotein; NAWM = normal-appearing white matter in the medulla, midbrain, and cerebellum.

proteolipid protein (PLP), antimyelin oligodendrocyte glycoprotein (MOG), microglia/macrophages (anti-Ki-M1P), T cells (anti-CD3; Dako, Copenhagen, Denmark), B cells (anti-CD79a; Dako), plasma cells (antihuman immunoglobulin G; Dako), and anti-glial fibrillary acidic protein (Dako).

For in situ hybridization, digoxigenin-labeled riboprobes specific for PLP mRNA were used. The source and specificity of the probes, labeling techniques, and methods of in situ hybridization have been described previously.[8]

The in situ tailing (IST) protocol has been described previously.[9] Oligodendrocytes were identified by double immunocytochemistry for MOG as described above.

Morphometry

Numbers of oligodendrocytes (MOG or PLP mRNA), apoptotic oligodendrocytes (MOG or CNPase and IST) and macrophages/microglia (Ki-M1P) stained per square unit of tissue were determined on serial sections in at least 10 standardized microscopic fields of 10,000μm^2 each, defined by an ocular morphometric grid. Values in the table and figures represent the number of cells per square millimeter. Relative axonal density was determined in sections stained with Bielschowsky's silver impregnation by point sampling using a 25-point eyepiece (Zeiss, Oberkochen, Germany), as described previously.[10]

Results

Macroscopically, cerebral hemispheres were grayish and appeared cystic. Myelin staining revealed a massively reduced staining intensity (Fig 1A); a prominent loss of axons was seen (Table; see Fig 1B and D). U-fibers, the corpus callosum, and the internal capsule were largely spared. A more detailed analysis revealed the presence of thin myelin sheaths in the LFB and myelin protein stains (see Fig 1C). Oligodendrocytes were reduced in number (see Fig 1E and Table), although a considerable number of oligodendrocytes were still present; PLP mRNA-expressing oligodendrocytes were increased over MOG-positive cells. There was prominent microglia activation in the gray matter and a mixed microglia/macrophage infiltrate in the cerebral lesions (see Fig 1F). T lymphocytes or B cells were completely absent. Similar pathological changes were seen in the autopsy specimens of cerebral hemispheres from the male relative of the patient, who died 25 years previously.

A quite different type of lesion pathology was observed in the pontine white matter. LFB and MBP staining revealed a demyelinated lesion with prominent macrophage infiltration in the absence of T or B cells. There was minor axonal loss (see Table); whether this was part of the initial disease process or due to Wallerian degeneration of the descending fiber tracts is not clear. Higher magnifications revealed macrophages with LFB-, MBP-, and MOG-positive myelin degradation products (Fig 2A and B), indicating recent and active demyelination.[11] In these areas, oligodendrocytes were significantly reduced (see Fig 2C and Table). The IST reaction revealed numerous oligodendrocytes with DNA fragmentation (see Fig 2D). These dying cells showed all of the morphological signs of apoptosis (see Fig 2E and F).

Pathological findings were also observed in the white matter, which appeared normal in the myelin stains (see Fig 2G and H). A high number of PLP mRNA-expressing oligodendrocytes were present (see Fig 2I). There were, however, MOG-positive oligodendrocytes with all of the morphological characteristics of apoptosis (see Fig 2K and Table). In Bielschowsky's silver impregnation, there were no axonal bulbs detected as signs of acute axonal damage.

Discussion

Myelinopathia centralis diffusa, or vanishing white matter disease, is a recently defined leukoencephalopathy of childhood with characteristic clinical and neuroradiological features. The pathogenesis of this disease remains unknown. Increasing numbers of oligodendrocytes have been described in two studies.[3,7] The present case clearly revealed primary destruction of mature oligodendrocytes via apoptosis in early lesion formation, which was followed by recruitment of progenitor cells expressing PLP mRNA.

The morphological features of oligodendrocyte death in combination with the detection of DNA fragmentation suggest that apoptosis is critically involved in oli-

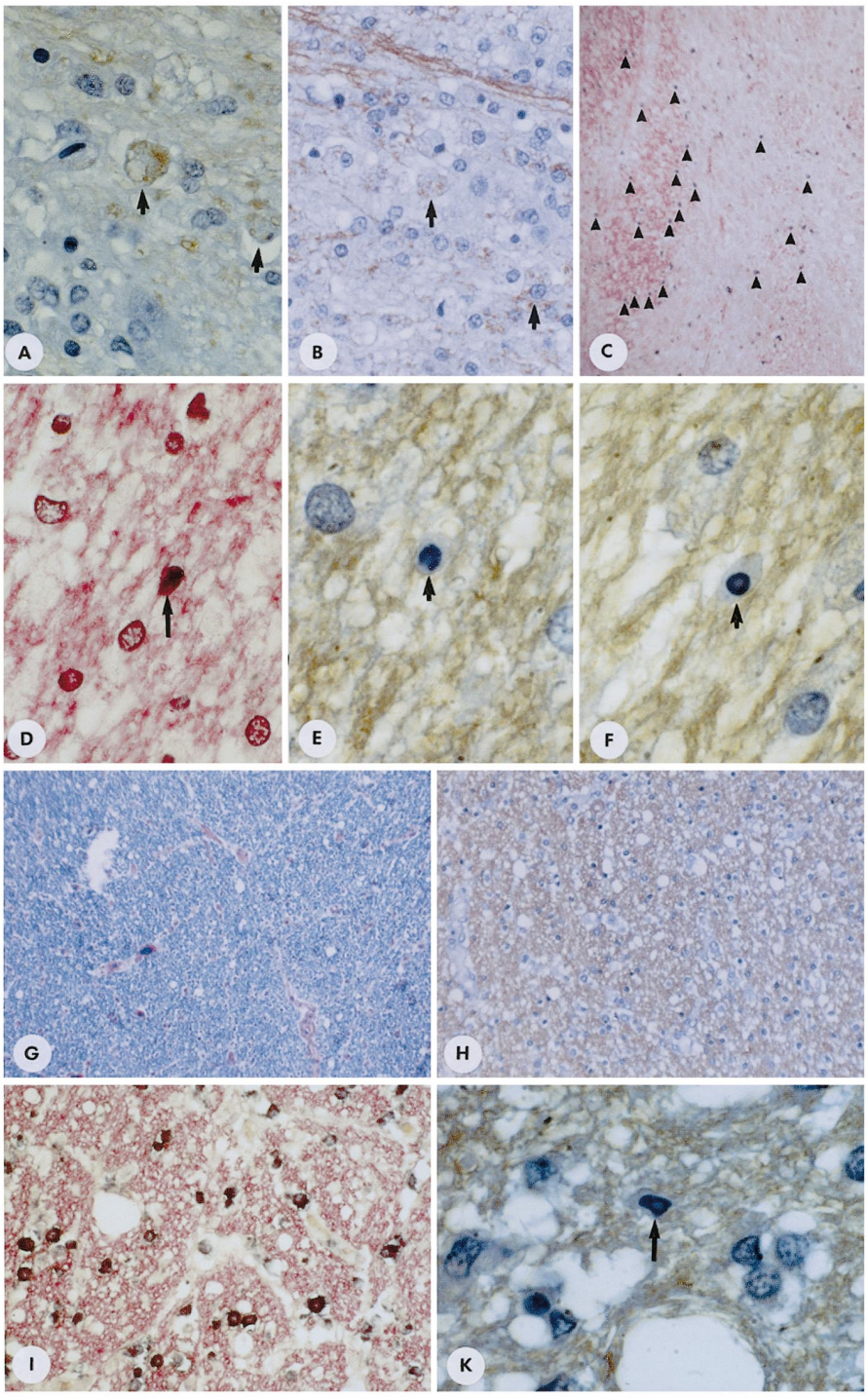

Fig 2. (A–F) Pathology of the active demyelinating brainstem lesion. (A and B) Macrophages (arrows) *contain (A) myelin oligodendrocyte glycoprotein (MOG)$^+$ (A), and myelin basic protein (MBP)$^+$ (B) degradation products (immunocytochemistry for MOG and MBP). (C) The number of proteolipid protein (PLP) mRNA–expressing oligodendrocytes* (arrowheads) *is reduced in the demyelinated area* (right) *compared with the normal-appearing white matter* (left). *(D) MOG$^+$ oligodendrocyte* (arrow) *with DNA fragmentation (immunocytochemistry for MOG in red, in situ tailing in black). (E and F) MOG$^+$ oligodendrocytes* (arrows) *stained at the surface showing chromatin condensation and margination characteristic of apoptosis. (G–K) Pathology of normal-appearing white matter. (G and H) Myelin appears normal with Luxol fast blue and periodic acid–Schiff stain (G) and by immunocytochemistry for MBP (H). (I) Numerous PLP mRNA–expressing oligodendrocytes are present (in situ hybridization for PLP in black, immunocytochemistry for PLP protein in red). (K) MOG$^+$ oligodendrocyte* (arrow) *with the typical morphology of apoptosis in normal white matter.*

godendrocyte degeneration in myelinopathia centralis diffusa. Apoptotic oligodendrocyte degeneration is a hallmark of different demyelinating conditions, including autoimmune-mediated demyelination,[11] virus-induced myelin destruction,[12] toxic oligodendrocyte damage,[13] as well as myelin protein deficiency.[14] The autoimmune features of demyelination were not observed in the present case. Clinically and histopathologically, infectious disorders and the known hereditary leukoencephalopathies or hypomyelinating diseases have been excluded. The morphological features presented here suggest severe damage of the oligodendrocyte that has just finished maturation and myelination. In most cases reported in the literature, the disease starts at this age (16–17 years), although later age of onset has been described.[7]

Detection of oligodendrocyte apoptosis in the absence of inflammation leaves the field open for possible pathogenetic mechanisms. Macrophage/microglia-derived cytotoxic mediators such as tumor necrosis factor (TNF)-α or lymphotoxin are known to induce oligodendrocyte apoptosis, and overexpression of TNF-α in transgenic mice results in oligodendrocyte apoptosis and primary demyelination.[15] Thus, microglial dysregulation could lead to the morphological changes observed in this disease. Growth factors are important for the development of oligodendrocytes. However, when applied at the inappropiate time and maturation state, these factors trigger oligodendrocyte apoptosis.[16] Another pathogenetic mechanism involved may be alterations in the cell death program of oligodendrocytes. Overexpression of the protooncogene *p53*, for example, induces programmed cell death of oligodendrocytes.[17]

Damage to axons is severe in the disease, but it seems to occur in the later stages of the lesion and is not part of the initial events. This is in contrast to inflammatory demyelinating lesions, in which axons are destroyed initially.[10] Remyelinated axons seem to be protected from further damage,[18] indicating that trophic support by oligodendrocytes may prevent axonal degeneration. Such a mechanism has been suggested in experimental animal models deficient in myelin proteins.[19] The continuous depletion of mature oligodendrocytes in vanishing white matter disease may therefore predispose for secondary axonal destruction.

The familial predisposition of the disease suggests a genetic background. Recently, the locus of the gene for the disease was found on chromosome 3q27.[20] Further studies will identify the genes responsible for the pathogenesis of myelinopathia centralis diffusa, or vanishing white matter disease.

References

1. Hanefeld F, Holzbach U, Kruse B, et al. Diffuse white matter disease in three children: an encephalopathy with unique features on magnetic resonance imaging and proton magnetic resonance spectroscopy. Neuropediatrics 1993;24:244–248.
2. van der Knaap MS, Barth PG, Gabreels FJM, et al. A new leukoencephalopathy with vanishing white matter. Neurology 1997;48:845–855.
3. Rodriguez D, Gelot A, della Gaspera B, et al. Increased density of oligodendrocytes in childhood ataxia with diffuse central hypomyelination (CACH) syndrome: neuropathological and biochemical study of two cases. Acta Neuropathol 1999;97: 469–480.
4. Schiffmann R, Moller JR, Trapp BD, et al. Childhood ataxia with diffuse central nervous system hypomyelination. Ann Neurol 1994;35:331–340.
5. Deisenhammer E, Jellinger K. Cavitating neutral fat leukodystrophy with recurrent course. Neuropediatrics 1976;7:111–121.
6. Watanabe I, Muller J. Cavitating "diffuse sclerosis." J Neuropathol Exp Neurol 1967;26:437–455.
7. van der Knaap MS, Kamphorst W, Barth PG, et al. Phenotypic variation in leukoencephalopathy with vanishing white matter. Neurology 1998;51:540–547.
8. Breitschopf H, Suchanek G, Gould RM, et al. In situ hybridization with digoxigenin-labeled probes: sensitive and reliable detection method applied to myelinating rat brain. Acta Neuropathol 1992;84:581–587.
9. Brück Y, Brück W, Kretzschmar HA, Lassmann H. Evidence for neuronal apoptosis in pontosubicular neuron necrosis. Neuropathol Appl Neurobiol 1996;22:23–29.
10. Bitsch A, Schuchardt J, Bunkowski S, et al. Axonal injury in multiple sclerosis. Correlation with demyelination and inflammation. Brain 2000;123:1174–1183.
11. Lucchinetti C, Brück W, Parisi J, et al. Heterogeneity of multiple sclerosis lesions: implications for the pathogenesis of demyelination. Ann Neurol 2000;47:707–717.
12. Barac-Latas V, Suchanek G, Breitschopf H, et al. Patterns of oligodendrocyte pathology in coronavirus-induced subacute demyelinating encephalomyelitis in the Lewis rat. Glia 1997;19: 1–12.
13. Ludwin SK, Johnson ES. Evidence for a "dying-back" gliopathy in demyelinating disease. Ann Neurol 1981;9:301–305.
14. Lassmann H, Bartsch U, Montag D, Schachner M. Dying-back oligodendrogliopathy: a late sequel of myelin-associated glycoprotein deficiency. Glia 1997;19:104–110.
15. Akassoglou K, Bauer J, Kassiotis G, et al. Oligodendrocyte apoptosis and primary demyelination induced by local TNF/p55TNF receptor signaling in the central nervous system of transgenic mice. Am J Pathol 1998;153:801–813.
16. Muir DA, Compston DAS. Growth factor stimulation triggers apoptotic cell death in mature oligodendrocytes. J Neurosci Res 1996;44:1–11.
17. Eizenberg O, Faber-Elman A, Gottlieb E, et al. Direct involvement of p53 in programmed cell death of oligodendrocytes. EMBO J 1995;14:1136–1144.
18. Kornek B, Storch MK, Weissert R, et al. Multiple sclerosis and chronic autoimmune encephalomyelitis. A comparative quantitative study of axonal injury in active, inactive, and remyelinated lesions. Am J Pathol 2000;157:267–276.
19. Griffiths I, Klugmann M, Anderson T, et al. Axonal swellings and degeneration in mice lacking the major proteolipidprotein of myelin. Science 1998;280:1610–1613.
20. Leegwater PAJ, Könst AAM, Kuyt B, et al. The gene for leukoencephalopathy with vanshing white matter is located on chromosome 3q27. Am J Hum Genet 2001;65:728–734.

A Novel Deafness/Dystonia Peptide Gene Mutation that Causes Dystonia in Female Carriers of Mohr-Tranebjaerg Syndrome

Russell H. Swerdlow, MD, and G. Frederick Wooten, MD

Sex-linked male deafness and dystonia (Mohr-Tranebjaerg syndrome) arises from mutation of the deafness/dystonia peptide *(DDP)* gene. We describe a novel guanine deletion at nucleotide 108 of the *DDP* gene in a family with Mohr-Tranebjaerg syndrome, which terminates this 97–amino acid protein at codon 25. Unlike previously reported kindreds, carrier females in this family also manifest dystonias, including torticollis and writer's cramp. A family history of male deafness should alert clinicians to the possibility of *DDP* mutation in women with focal dystonias.

Ann Neurol 2001;50:537–540

A sex-linked sensorineural deafness disorder (DFN-1) was described in 1960 by Mohr and Mageroy.[1] Subsequent observations of concomitant dystonia in DFN-1 males defined an expanded phenotype, the Mohr-Tranebjaerg syndrome (MTS).[2,3] In 1995, Tranebjaerg and colleagues[2] established linkage in an MTS kindred to Xq21.3-Xq22. The following year, Jin and colleagues[4] implicated mutation of a gene they named the dystonia/deafness peptide *(DDP)* gene. Three unrelated kindreds with three different mutations were initially described, followed by a unique de novo mutation in a male child.[4,5] Another mutation of the *DDP* gene was also discovered in a family with the phenotypically similar Jensen syndrome,[6,7] which was then reclassified as part of the MTS spectrum.[8]

We now describe a kindred with X-linked deafness/dystonia and a novel *DDP* mutation. In addition to the presence of a previously undescribed mutation, this kindred is unique in that female carriers also manifest dystonia syndromes.

From the Department of Neurology and the Center for the Study of Neurodegenerative Diseases, University of Virginia Health System, Charlottesville, VA.

Received Apr 30, 2001, and in revised form Jun 19. Accepted for publication Jun 23, 2001.

Published online Aug 2, 2001; DOI: 10.1002/ana1160

Address correspondence to Dr Swerdlow, Box 394, Department of Neurology, McKim Hall, 1 Hospital Drive, Charlottesville, VA 22908. E-mail: rhs7e@virginia.edu

Subjects and Methods

The proband is a 30-year-old male previously diagnosed with congenital deafness (Subject IV:2, Fig 1). At age 28 years, he developed progressively worsening involuntary head-and-neck movements. Our examination revealed generalized dystonia and a markedly hypertrophied right sternocleidomastoid. He held his head deviated to the left with a tilt to the right. Intermittent, involuntary contractions of the right sternocleidomastoid flexed his right ear onto his shoulder. There was scoliosis concave to the right. Cranial nerve examination revealed frequent facial grimacing and blepharospasm. Intermittent torsional contractions occurred in all four limbs. Muscle tone was normal between paroxysms of dystonic contractions.

The proband's mother (Subject III:9, see Fig 1) reported head shaking, chronic neck muscle pain, and writer's cramp since age 25 years. Examination revealed repetitive horizontal head jerks with brief, palpable, involuntary contractions of the bilateral sternocleidomastoids and other neck muscles. Hearing was grossly normal.

Two female siblings of the proband were examined. Subject IV:4 was normal. Subject IV:3 reported the onset of head shaking in her late teens and writer's cramp in her mid-twenties. On examination, she manifested hypertrophy of both sternocleidomastoid muscles with head deviation to the right, prolonged jerky horizontal head shaking, and frequent, palpable, semirhythmic contractions of multiple neck muscles.

A brother of the proband (IV:1, see Fig 1), was by report neurologically normal. The proband's mother reported that 2 half-brothers (different father, common mother) were deaf at the time of, or perhaps shortly after, birth. One of these brothers (III:11) developed a generalized dystonic disorder in his late twenties, blindness in his early fifties, and dementia in his late fifties. He died at age 63 years. The other brother (III:12) died at age 22 years without having developed dystonia. The proband's maternal grandmother was said to be normal, but the maternal great-grandmother's (I:1) head shook. A sister of the proband's grandmother had 2 sons (III:2 and III:3) who were deaf and developed generalized dystonia as adults.

Genetic analyses were performed under a protocol approved by the University of Virginia Investigational Review Board. Following informed consent, blood samples were obtained from each of the 4 subjects studied. DNA extractions were done with a QIAamp DNA minikit (Qiagen, Valencia, CA). Taq/Pwo polymerase (Roche Diagnostics, Indianapolis, IN) and a GeneAmp9600 were used for polymerase chain reaction (PCR) amplifications of the 2-exon *DDP* gene. The primers used were previously described by Jin and colleagues[4] with minor modification. The exon 1 primers were 5′-GCGGAGTTCGTCTCTGCAAGC-3′ (upper primer) and 5′-GTAGGTACAGTGTTCAGGTC-3′ (lower primer). The exon 2 primer sequences were 5′-CTAAGCAACAAAAAGGGAC-3′ (upper primer) and 5′-GTTCACTGGCTAGATTCC-3′ (lower primer). Thirty cycles were run for each reaction, with an annealing temperature of 62°C and extension time of 60 seconds.

PCR products were purified with a QIAquick kit (Qiagen). Dideoxynucleotide chain termination sequencing of exon 1 and exon 2 amplicons from the proband and his mother were performed using an Applied Biosystems (model

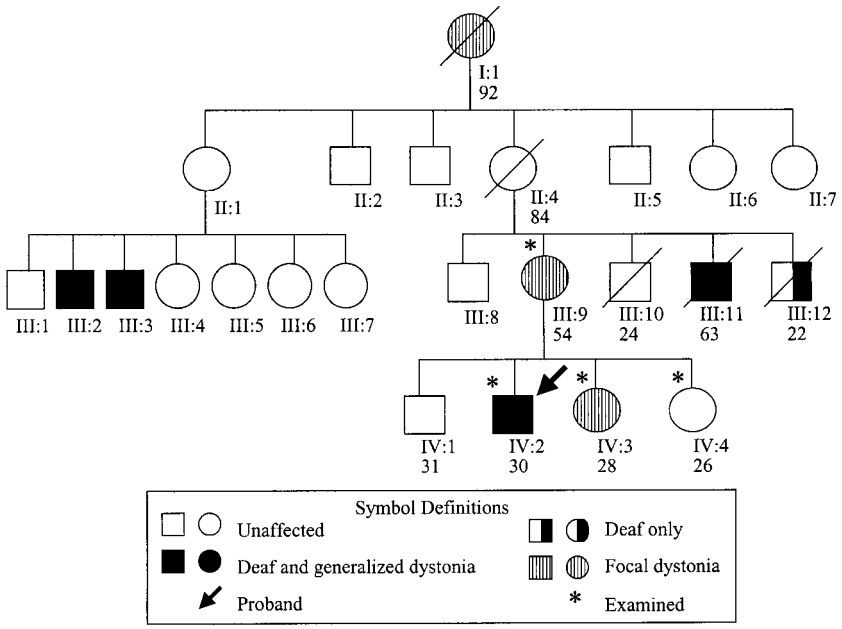

Fig 1. A family with dystonia with or without deafness over multiple generations. In this family, deafness appears to represent an X-linked recessive trait.

Fig 2. Deafness/dystonia peptide (DDP) *gene exon 1 chromatograms from the male proband and his mother. (A) Chromatogram from the male proband shows a guanine deletion at nucleotide 108. (B) Chromatogram from the proband's mother reveals that she is heterozygous and indicates the presence of both a normal allele and an allele with a deletion at nucleotide 108.*

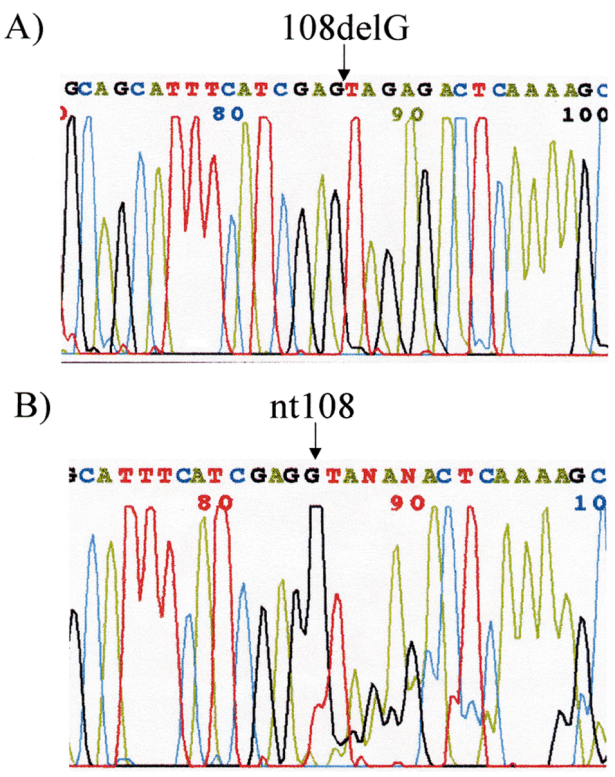

377; Foster City, CA) sequencer. Sequencing reactions contained 8pmol of the same primers employed in the PCR amplification and 20ng/100 bp of exon 1 and exon 2 product. Sequence data were compared to those reported by Jin and colleagues[4] and to those reported for the *DDP* cDNA in Genbank (accession U66035).

For restriction fragment length polymorphism assays, 700 to 800ng of purified exon 1 PCR product from each subject were incubated with MnlI (New England Biolabs, Beverly, MA); 350 to 400ng of each digestion product were electrophoresed on a 4% agarose gel containing ethidium bromide (E-Gel; Invitrogen, Carlsbad, CA).

Results

The extended kindred is illustrated in Figure 1. By report, some affected males displayed deafness from birth, which is somewhat unique because deafness in other reported MTS families arose after attainment of early childhood language milestones.[9] We can neither confirm nor dispute the accuracy of the congenital deafness reports for Subject IV:2 and possibly III:11 and III:12.

For genetic studies of the DDP gene, the DDP exon 2 sequence from the proband did not differ from the reported sequence.[4] In exon 1, the proband demonstrated a silent A→G transition at nt 86. The mother was homozygous for this polymorphism. The proband's sequence also revealed a G deletion at nt 108, for which the mother was heterozygous (Fig 2). This 108delG mutation converts the 25th codon of the protein, which typically codes for valine, to a stop codon.

The restriction enzyme MnlI cuts 7 nucleotides downstream of 5′-CCTC-3′ sequences and 6 nucleotides upstream of 3′-GGAG-5′ sequences. The wild type exon 1 amplicon contains three such sequences, which determine cuts at nt 53, 98, and 163 of the wild type exon 1

amplicon (Fig 3). Additional 5′-CCTC-3′ sequences are present at nt 49–52 and nt 55–58. The nt 49–52 5′-CCTC-3′ determines a cut at nt 59 that can remove the nt 55–58 5′-CCTC-3′ from the 5′ end of the downstream fragment. Doing so results in a 39 bp downstream fragment. Alternatively, the cut at nt 53 can neutralize the 49–52 5′-CCTC-3′ site so that the 5′ end of the downstream fragment is determined by the nt 55–58 5′-CCTC-3′. In this scenario, the 5′ end of the downstream fragment begins at nt 65 (yielding a 33 bp downstream fragment). The 108delG mutation disrupts a 3′-GGAG-5′ sequence and eliminates the cut at nt 98. Addition of the 33 and 39 bp fragments upstream of nt 98 to the 64 bp fragment that is downstream to it creates unique 96 and 102 bp fragments.

The results of the MnlI restriction digests are shown in Figure 3. The proband's pattern was consistent with the absence of a wild type allele and the presence of the 108delG mutation. The proband's asymptomatic sister showed only the wild type pattern, indicating that she is not a 108delG carrier. The proband's mother and symptomatic sister possessed both wild type and 108delG alleles.

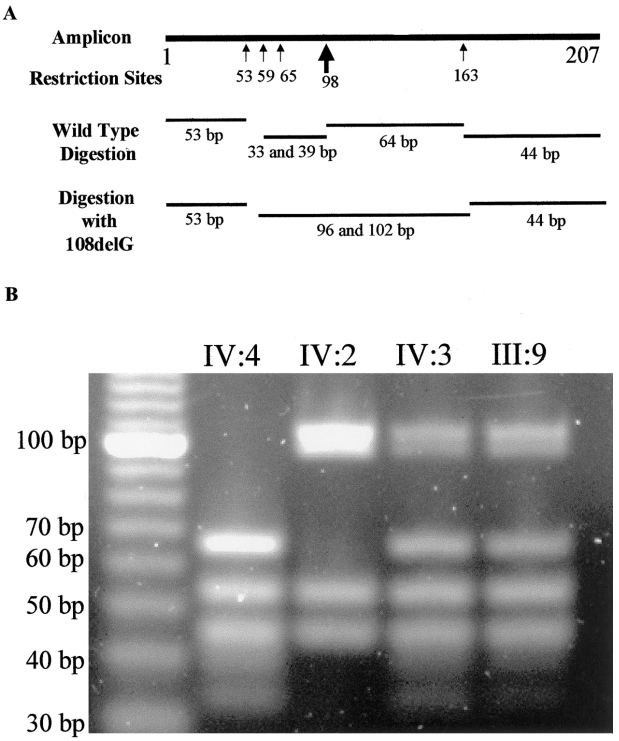

Fig 3. Deafness/dystonia peptide (DDP) *restriction by MnlI. (A) MnlI restriction sites are shown for the 207 bp exon 1 amplicon (see text). The 108delG mutation eliminates the restriction site that is normally present at nucleotide 98. (B) MnlI restrictions of* DDP *exon 1 from symptomatic and asymptomatic members of the Mohr-Tranebjaerg syndrome kindred. The first lane is a molecular weight marker showing 10 bp increments.* Lane 2 *is from the asymptomatic female Subject IV:4 (a sister of the proband) and shows the expected wild-type bands. The proband (Subject IV:2), who is deaf and severely dystonic, displays a hemizygous mutation* (lane 3). *This is indicated by 108delG-related loss of an MnlI restriction site.* Lane 4 *is from the proband's other sister (Subject IV:3) with focal dystonias and reveals the presence of both 108delG and wild-type alleles.* Lane 5 *is from the mother (Subject III:9) of the 3 siblings. She also suffers from focal dystonias and is a heterozygous carrier of the 108delG mutation.*

Discussion

This 108delG mutation converts the 97–amino acid DDP to a 24–amino acid peptide. Regarding deafness, the mutation is recessive as female carriers do not complain of hearing loss. The mutation's effects on movement, however, are best characterized as dominant, with greater penetrance in males. It is conceivable that some women who present with seemingly sporadic idiopathic dystonias actually possess *DDP* mutation. Family histories of female patients with dystonia should carefully assess for the presence of deafness, cerebral palsy, or early death in male relatives.

Males with the 108delG mutation manifest generalized dystonia, while females experience focal dystonia syndromes. Possible explanations for this include the potential ability of the normal allele to provide an ameliorative effect despite its inactivation or X-chromosome inactivation that leads to a mosaic pattern of mutational expression. In our opinion, the latter explanation is more probable.

Previously described MTS *DDP* gene mutations include a total gene deletion, a 10 bp deletion starting at nt 183 in exon 2, a 151delT in exon 1, a C233G transition in exon 2, and a G105T transversion in exon 1.[4,5,7] The 108delG mutation we now describe should yield a protein similar to that of the G105T mutation (which leads to translation termination at the adjacent upstream codon). These earlier reports did not describe movement disorder as a clinical manifestation in carrier females. It is unclear why one *DDP* gene mutation (108delG) might affect movement in a dominant fashion, while a neighboring mutation or total gene deletion does not. One observation potentially relevant to this issue is that *DDP* mutation appears to skew X-chromosome inactivation patterns[10]; perhaps different mutations can variably skew X-chromosome inactivation in phenotypically relevant ways.

In 1999, homology of DDP to a family of peptides responsible for mitochondrial protein translocation was noted.[11] Its counterpart in yeast is the mitochondrial protein Tim 8p, and DDP was recently renamed translocase of the inner mitochondrial membrane (TIMM) 8a.[11,12] Specific mitochondrial DNA mutations are also accepted as primary causes of both deafness and dystonia.[13–15] The finding of TIMM protein mutation

as the apparent cause of deafness and dystonia in this kindred emphasizes the relevance of mitochondria to disorders of sensorineural hearing and movement.

This study was supported by grants from the National Institute of Aging, the National Institute of Neurologic Diseases and Stroke, and the American Parkinson's Disease Association.

We are grateful to Dr Lil Currie for assistance with Figure 1.

References

1. Mohr J, Mageroy K. Sex-linked deafness of a possibly new type. Acta Genet Stat Med 1960;10:54–62.
2. Tranebjaerg L, Schwartz C, Eriksen H, et al. A new X linked recessive deafness syndrome with blindness, dystonia, fractures, and mental deficiency is linked to Xq22. J Med Genet 1995; 32:257–263.
3. Scribanu N, Kennedy C. Familial syndrome with dystonia, neural deafness, and possible intellectual impairment: clinical course and pathological findings. Adv Neurol 1976;14: 235–243.
4. Jin H, May M, Tranebjaerg L, et al. A novel X-linked gene, DDP, shows mutations in families with deafness (DFN-1), dystonia, mental deficiency and blindness. Nat Genet 1996;14: 177–180.
5. Tranebjaerg L, Hamel BCJ, Gabreels FJM, et al. A de novo missense mutation in a critical domain of the X-linked DDP gene causes the typical deafness–dystonia–optic atrophy syndrome. Eur J Hum Genet 2000;8:464–467.
6. Jensen PKA, Reske-Nielsen E, Hein-Sorensen O, Warburg M. The syndrome of opticoacoustic nerve atrophy with dementia. Am J Med Genet 1987;28:517–518.
7. Tranebjaerg L, Schwarz C, Huggins K, et al. Jensen syndrome is allelic to Mohr-Tranebjaerg syndrome and both are caused by stop mutations in the DDP gene. Am J Hum Genet 1997; 51(Suppl):A349.
8. Lubs H, Chiurazzi J, Arena J, et al. XLMR genes: update 1998. Am J Med Genet 1999;83:237–247.
9. Tranebjaerg L, Jensen PKA, van Ghelue M. X-linked recessive deafness-dystonia syndrome (Mohr-Tranebjaerg syndrome). In: Kitamura K, Steel KP, eds. Genetics in otorhinolaryngology. Advances in otorhinolaryngology, vol 56. Basel: Karger; 2000: 176–180.
10. Plenge RM, Tranebjaerg L, Jensen KA, et al. Evidence that mutations in the X-linked DDP gene cause incompletely penetrant and variable skewed X inactivation. Am J Hum Genet 1999; 64:759–767.
11. Koehler CM, Leuenberger D, Merchant S, et al. Human deafness dystonia syndrome is a mitochondrial disease. Proc Natl Acad Sci U S A 1999;96:2141–2146.
12. Jin H, Kendall E, Freeman TC, et al. The human family of deafness/dystonia peptide (DDP) related mitochondrial import proteins. Genomics 1999;61:259–267.
13. Jun AS, Brown MD, Wallace DC. A mitochondrial DNA mutation at nucleotide pair 14459 of the NADH dehydrogenase subunit 6 gene associated with maternally inherited Leber hereditary optic neuropathy and dystonia. Proc Natl Acad Sci U S A 1994;91:6206–6210.
14. Wallace DC, Murdock DG. Mitochondria and dystonia: the movement disorder connection? Proc Natl Acad Sci U S A 1994;96:1817–1819.
15. Simon DK, Johns DR. Mitochondrial disorders: clinical and genetic features. Annu Rev Med 1999;50:111–127.

Multisystem Disorder Associated with a Missense Mutation in the Mitochondrial Cytochrome *b* Gene

Flemming Wibrand, PhD,[1] Kirstine Ravn, MSc,[2] Marianne Schwartz, PhD,[2] Thomas Rosenberg, MD,[3] Nina Horn, PhD,[1] and John Vissing, MD, PhD[4]

Mitochondrial cytochrome *b* mutations have been reported to have a homogenous phenotype of pure exercise intolerance. We describe a novel mutation in the cytochrome *b* gene of mitochondrial DNA (A15579G) associated with a selective decrease of muscle complex III activity in a patient who, besides severe exercise intolerance, also has multisystem manifestations (deafness, mental retardation, retinitis pigmentosa, cataract, growth retardation, epilepsy). The point mutation is heteroplasmic in muscle (88%) and leukocytes (15%), and changes a highly conserved tyrosine to cysteine at amino acid position 278.

Ann Neurol 2001;50:540–543

Complex III (ubiquinol:ferricytochrome-*c* oxidoreductase, EC 1.10.22), the central segment of the respiratory chain, is composed of 11 subunits. Only one of these, cytochrome *b* (cyt *b*), is encoded by mitochondrial DNA (mtDNA). The first mutation in the cyt *b* gene was described in 1996, in a patient presenting with exercise intolerance and reduced complex III activity in muscle.[1] Since then, 8 patients with pathogenic cyt *b* mutations and a similar phenotype have been identified.[2–5] Based on these findings, it has been proposed that mutations in this mitochondrial gene are associated with a pure myopathic phenotype involving exercise intolerance, sometimes accompanied by weakness or myoglobinuria.[3,4] We describe a novel missense

From the [1]John F. Kennedy Institute, Glostrup and [2]Department of Clinical Genetics, National University Hospital, Rigshospitalet, Copenhagen; [3]National Eye Clinic for the Visually Impaired, Hellerup; and [4]Department of Neurology, National University Hospital, Rigshospitalet, Copenhagen, Denmark.

Received Mar 6, 2001, and in revised form Jun 25. Accepted for publication Jun 26, 2001.

Published online Aug 23, 2001; DOI: 10.1002/ana.1224

Address correspondence to Dr Vissing, Neuromuscular Clinic, Department of Neurology 2082, National University Hospital, Rigshospitalet, Blegdamsvej 9, DK-2100 Copenhagen, Denmark. E-mail: vissing@rh.dk

mutation in the cyt *b* gene in a patient with multiorgan involvement.

Case Report

The patient is a 19-year-old woman. At age 6 years, bilateral central hearing loss was detected, and the condition progressed to deafness at age 11 years. At age 15 years, a cochlear stimulator was implanted. At age 10 years, it was noted that she had exercise intolerance, cognitive dysfunction, and growth retardation. Neuroendocrine investigations indicated relative inhibition of pituitary growth hormone secretion, and she was treated with growth hormone injections. Due to deficient development of secondary sexual characteristics, the patient was also treated with estrogens. At age 19 years, neuropsychological tests indicated cognitive function corresponding to a 14-year-old girl. Nausea, headaches, and occasional vomiting accompanied low-intensity exercise. Echocardiography was normal. Eye examination revealed bilateral cataracts and a retinal rod and cone dystrophy (atypical retinitis pigmentosa). Binocular visual acuity was 0.4. No oculomotor deficiency was present. Manual muscle testing revealed diffuse muscle weakness of 4 to 4+ on the Medical Research Council score in all limbs. Cerebral magnetic resonance images (MRIs) at ages 11 and 15 years were normal. Plasma creatine kinase, carnitine, aminotransferase, and glucose levels were normal. Lactate concentrations were elevated in the blood (range, 4 to 8mmol/L) and cerebrospinal fluid (8.8mmol/L). The patient developed epilepsy at the age of 19 years. She has been treated with coenzyme Q10 (60mg daily) and ascorbic acid (500mg daily) for several years without apparent effect. The 2 parents and a younger sister showed no signs of neuromuscular disease. The patient was further evaluated with a cycle ergometry test and a needle biopsy from the left lateral vastus muscle.

Biochemical Investigations

Mitochondrial enzyme activities were measured in postnuclear supernatants of frozen muscle, as described previously.[6,7] The activities of respiratory chain enzyme complexes were expressed relative to the activity of the matrix enzyme citrate synthase, to correct for different mitochondrial contents.

Molecular Genetic Investigations

To prepare templates for mtDNA sequencing, the entire mtDNA was amplified by polymerase chain reaction (PCR) in two segments with the following 20mer primers corresponding to the mtDNA position: L-strand 336/H-strand 5745, L-strand 5756/H-strand 282, using the Expand Long Template PCR System (Boehringer-Mannheim, Mannheim, Germany).[8] All tRNA genes as well as the cyt *b* gene were sequenced using an automated DNA sequencer (model 310) and fluorescent dye-labeled ddNTP chain terminators (Bigdye Sequencing System; Applied Biosystems, Foster City, CA). Sequencing primers were spaced by approximately 400 nucleotides, to cover these genes in overlapping fragments. PCR-restriction fragment length polymorphism (RFLP) analysis was performed to detect the A-to-G transition at nt 15579. A 20mer light-strand primer corresponding to positions 15471 to 15490 was used in combination with a mismatch heavy-strand primer, corresponding to the mtDNA position 15580 to 15601 (5′-AGGGACGGATCGGAGAATTGCG-3′). The mismatch primer creates a HinPI restriction site, which is not present in the wild type mtDNA. The relative proportions of mutant and wild type mtDNA were determined by solid-phase mini-sequencing.[9]

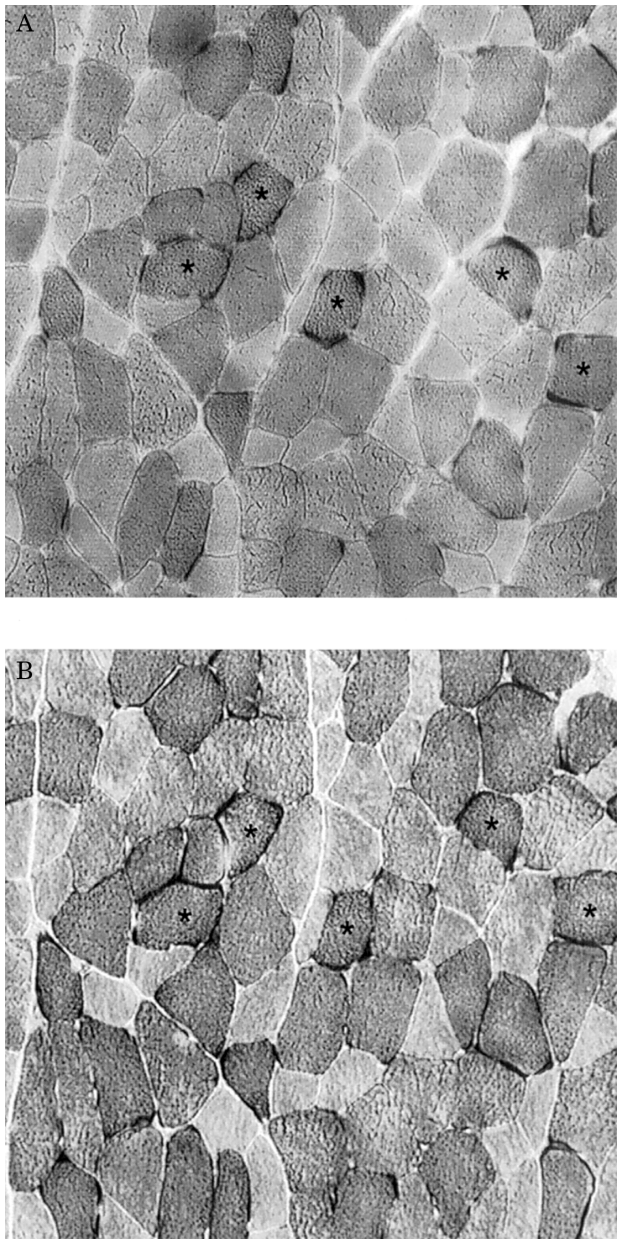

*Fig 1. Trichrome (A) and cytochrome-*c *oxidase (B) staining of serial sections of vastus lateralis muscle. Ragged red fibers* (asterisks) *seen in the trichrome stain also stain intensely for cytochrome-*c *oxidase.*

Results

The patient exercised for 6 minutes at a workload of 10W on a cycle ergometer (MedGraphics, CPE 2000; St Paul, MN) until severe nausea and fatigue devel-

Table. Activities of Mitochondrial Enzymes in Skeletal Muscle

	Patient	Controls (mean ± SD)[a]
NADH-decylubiquinone oxidoreductase (complex I)	0.25	0.28 ± 0.05 (0.21–0.34)
Succinate-decylubiquinone oxidoreductase (complex II)	0.21	0.28 ± 0.05 (0.20–0.35)
Decylubiquinol-cytochrome-*c* oxidoreductase (complex III)	0.05	0.85 ± 0.30 (0.46–1.38)
Cytochrome-*c* oxidase (complex IV)	3.29	3.20 ± 0.89 (1.93–4.68)
Citrate synthase	63.00	204.00 ± 73.00 (67.00–309.00)

Enzyme activity is expressed as milliunits per milliunits citrate synthase. Citrate synthase activity is expressed as milliunits per milligrams protein.
[a]13 age-matched individuals.

oped. Maximum oxygen consumption was 9ml/min^{-1}/kg^{-1} (normal for age is 45ml/min^{-1}/kg^{-1}). Cubital venous blood lactate concentration was elevated at rest (7.0 mmol/L) and increased to 9.0 mmol/L after 5 minutes of exercise.

The muscle biopsy showed numerous (17%) ragged red fibers in the trichrome stain (Fig 1A). All fibers, including ragged red fibers, stained intensely for cytochrome-*c* oxidase (see Fig 1B). Enzyme analysis revealed decreased complex III activity (6% of control mean) and normal activities of the other respiratory chain complexes (Table).

The biochemical investigations prompted us to sequence the cyt *b* gene. This revealed an A-to-G transition at nt 15579, which causes substitution of a tyrosine with a cysteine at amino acid position 278 (Y278C). PCR-RFLP analysis (Fig 2) and minisequencing showed that the patient's muscle (88%) and leukocytes (15%) were heteroplasmic for the mutation. The mutation was absent in the healthy mother's leukocytes and in 50 controls. Analysis of the patient's tRNA genes did not reveal any mutations.

Fig 2. Polymerase chain reaction–restriction fragment length polymorphism analysis (HinPI) of the A15579G mutation using a mismatch primer. The mutant sequence introduces a HinPI site (112bp), whereas the normal (wild-type) sequence lacks the HinPI site (131bp). Lane 1 = *molecular weight marker. Lane* 2 = *patient's muscle. Lane* 3 = *patient's blood. Lane* 4 = *patient's mother's blood. Lanes* 5 *and* 6 = *controls.*

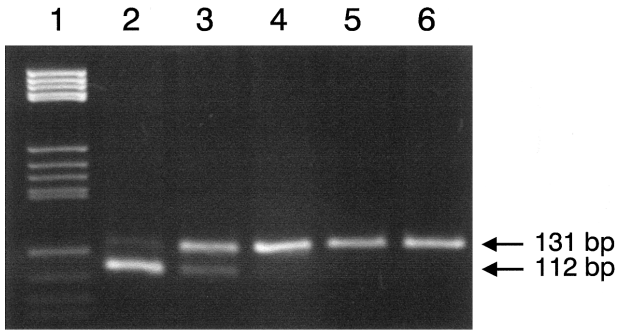

Discussion

We report on a patient with a missense mutation in the mitochondrial cyt *b* gene associated with a multisystem disorder. The mutation is pathogenic for the following reasons: (1) Biochemical studies revealed an isolated complex III deficiency in the patient's muscle tissue; (2) heteroplasmy was detected in muscle and leukocytes; (3) the mutation was absent in 50 controls and has not been reported as a polymorphic variant[10]; (4) the mutation was not found in the mother's leukocytes, suggesting a de novo mutation, which is characteristic of all cyt *b* mutations reported so far[11]; and (5) the mutation results in the substitution of tyrosine with cysteine at amino acid position 278, a radical change because tyrosine-278 is highly conserved throughout evolution[12] and is located within the ef helix, which is part of the quinol-oxidizing (Q_o) site.[13] Quinol oxidation occurs in a so-called bifurcated reaction, in which one electron is transferred to the Rieske iron-sulfur protein (ISP) and the other to the hemes of cyt *b*. Electron transfer to the ISP requires docking of the extrinsic domain of ISP at the interface on cyt *b*.[13,14] Tyrosine-278 lies at this interface and has been shown either to interact directly with the ISP[13] or to be part of a hydrophobic pocket, which most likely is involved when the quinone intermediate binds to the ISP.[14] The presence of a cysteine-278 instead of a tyrosine is likely to interfere with the docking process, thereby preventing formation of a quinone–ISP complex and blocking electron transfer.[13]

Since 1996, 9 patients with exercise intolerance have been found to harbor different pathogenic mutations in the cyt *b* gene.[1–5] Some also had weakness or myoglobinuria, but all symptoms were restricted to skeletal muscle. Based on these findings, it has been stated within the last 2 years, both in original articles[3,4] and in a review,[15] that cyt *b* mutations are associated with a homogeneous clinical phenotype of isolated myopathy. However, 4 patients with cyt *b* mutations and symptoms in one organ other than skeletal muscle have been identified; 2 had hypertrophic cardiomyopathy,[16,17] and 2 had progressive central nervous system

(CNS) involvement.[11,18] The patient described here has the most severe multiorgan manifestation seen so far in mitochondrial cyt *b* gene mutations. Besides exercise intolerance, it includes progressive hearing impairment, rod and cone dystrophy, cataract, cognitive impairment, and endocrine dysfunction resulting in delayed puberty, epilepsy, and growth retardation.

The distinguishing feature between patients presenting with pure muscle symptoms and those presenting with involvement of other organs is probably not related to the type of mutation because in both groups some had stop-codon mutations,[3–5,11] resulting in truncated cyt *b* protein, and others had deletions[4,18] or missense mutations[1,2,4,16,17] located within or close to one of the quinone-binding sites.[19] However, when comparing cyt *b* mutations associated with pure muscle symptoms and those with involvement of two or more organs, it appears that the conditions differ with respect to age at onset,[11] mutation load in muscle, presence of the mutation in tissues other than muscle,[11,20] and residual activity of complex III in muscle. When age at onset has been reported, patients with involvement of tissues other than muscle, including our patient, have onset at age 0 to 9 years,[11,16–18] whereas patients with pure myopathy have onset at age 10 to 30 years.[1–4] It also appears that the proportion of mutant mtDNA in muscle (or heart/liver) is higher in our patient and patients with heart or CNS involvement (87–95%, n = 5)[11,16–18] compared to the group with pure muscle symptoms (50–87%, n = 8).[1–4] In all patients with pure muscle symptoms, no mutation could be detected in leukocytes,[1–4] whereas the mutation was present in either leukocytes or other nonmuscle tissues of our patient and patients with heart or CNS involvement.[11,16–18] In addition, it appears that complex III (or II+III) activity in muscle extracts is lower in patients with other organ manifestations (5–9% of control means, n = 3)[11,18] than in those with pure myopathy (9–54% of control means, n = 7).[1–4]

The present report rejects the notion that cyt *b* mutations are associated with pure muscle symptoms, and indicates that mutations in the cyt *b* gene lead to a variety of phenotypes, as do most mutations in other mitochondrial genes. The findings also indicate that variable phenotypes may be explained by differences in the mutation load in muscle and other tissues.

References

1. Dumoulin R, Sagnol I, Ferlin T, et al. A novel gly290asp mitochondrial cytochrome *b* mutation linked to a complex III deficiency in progressive exercise intolerance. Mol Cell Probes 1996;10:389–391.
2. Andreu AL, Bruno C, Shanske S, et al. Missense mutation in the mtDNA cytochrome *b* gene in a patient with myopathy. Neurology 1998;51:1444–1447.
3. Andreu AL, Bruno C, Dunne TC, et al. A nonsense mutation (G15059A) in the cytochrome *b* gene in a patient with exercise intolerance and myoglobinuria. Ann Neurol 1999;45:127–130.
4. Andreu AL, Hanna MG, Reichmann H, et al. Exercise intolerance due to mutations in the cytochrome *b* gene of mitochondrial DNA. N Engl J Med 1999;341:1037–1044.
5. Pulkes T, Siddiqui A, Morgan-Hughes JA, et al. A novel heteroplasmic nonsense mutation in the mitochondrial cytochrome *b* gene associated with mitochondrial myopathy and complex III deficiency. Abstracts of the Fourth European Meeting on Mitochondrial Pathology, Cambridge, UK, 1999:P179.
6. Birch-Machin MA, Briggs HL, Saborido AA, et al. An evaluation of the measurement of the activities of complexes I–IV in the respiratory chain of human skeletal muscle mitochondria. Biochem Med Metab Biol 1994;51:35–42.
7. Krahenbuhl S, Talos C, Wiesmann U, et al. Development and evaluation of a spectrophotometric assay for complex III in isolated mitochondria, tissues and fibroblasts from rats and humans. Clin Chim Acta 1994;230:177–187.
8. Kleinle S, Wiesmann U, Superti-Furga A, et al. Detection and characterization of mitochondrial DNA rearrangements in Pearson and Kearns-Sayre syndromes by long PCR. Hum Genet 1997;100:643–650.
9. Suomalainen A, Syvanen AC. Quantitative analysis of RNA species by PCR and solid-phase minisequencing. Methods Mol Biol 1998;86:121–131.
10. MITOMAP: Human Mitochondrial Genome Database. Center for Molecular Medicine, Emory University, Atlanta, GA, U S A (http://www.gen.emory.edu/mitomap.html); 2001.
11. Keightley JA, Anitori R, Burton MD, et al. Mitochondrial encephalomyopathy and complex III deficiency associated with a stop-codon mutation in the cytochrome *b* gene. Am J Hum Genet 2000;67:1400–1410.
12. Esposti MD, De Vries S, Crimi M, et al. Mitochondrial cytochrome *b*: evolution and structure of the protein. Biochim Biophys Acta 1993;1143:243–271.
13. Crofts AR, Guergova-Kuras M, Huang LS, et al. Mechanism of ubiquinol oxidation by the bc1 complex: role of the iron sulphur protein and its mobility. Biochemistry 1999;38:15791–15806.
14. Iwata S, Lee JW, Okada K, et al. Complete structure of the 11-subunit bovine mitochondrial cytochrome bc1 complex. Science 1998;281:64–71.
15. Schapira AH. Mitochondrial disorders. Curr Opin Neurol 2000;13:527–532.
16. Valnot I, Kassis J, Chretien D, et al. A mitochondrial cytochrome *b* mutation but no mutations of nuclearly encoded subunits in ubiquinol cytochrome c reductase (complex III) deficiency. Hum Genet 1999;104:460–466.
17. Andreu AL, Checcarelli N, Iwata S, et al. A missense mutation in the mitochondrial cytochrome *b* gene in a revisited case with histiocytoid cardiomyopathy. Pediatr Res 2000;48:311–314.
18. De Coo IF, Renier WO, Ruitenbeek W, et al. A 4-base pair deletion in the mitochondrial cytochrome *b* gene associated with parkinsonism/MELAS overlap syndrome. Ann Neurol 1999;45:130–133.
19. Fisher N, Meunier B. Effects of mutations in mitochondrial cytochrome *b* in yeast and man. Eur J Biochem 2001;268:1155–1162.
20. Rana M, de Coo I, Diaz F, et al. An out-of-frame cytochrome *b* gene deletion from a patient with parkinsonism is associated with impaired complex III assembly and an increase in free radical production. Ann Neurol 2000;48:774–781.

Dextran Reduces Embolic Signals After Carotid Endarterectomy

Christopher R. Levi, MBBS, FRACP,[1]
Jacinda L. Stork, BA, BAppSci (Hons),[3]
Brian R. Chambers, MD, FRACP,[3]
Anne L. Abbott, MBBS, FRACP,[3]
Heather M. Cameron, RN,[3]
Anna Peeters, BSc (Hons), PhD,[2]
John P. Royle, FRACS, FACS,[3]
Andrew K. Roberts, FRACS, FACS,[3]
Gary Fell, MBBS, FRACS,[3]
Michael C. Hoare, MBBS, FRACS,[3]
Anthony T. W. Chan, Mmed (Surg), FRACS,[3]
and Geoffrey A. Donnan, MD, FRACP[3]

One hundred fifty patients undergoing carotid endarterectomy were randomly assigned to receive intravenous 10% dextran 40 or placebo. Transcranial Doppler monitoring of the ipsilateral middle cerebral artery 0 to 1 hour postoperatively detected embolic signals in 57% of placebo and 42% of dextran patients, with overall embolic signal counts 46% less for dextran ($p = 0.052$). Two to 3 hours postoperatively, embolic signals were present in 45% of placebo and 27% of dextran patients, with embolic signal counts 64% less for dextran ($p = 0.040$). We conclude that dextran reduces embolic signals within 3 hours of CEA.

Ann Neurol 2001;50:544–547

Carotid endarterectomy (CEA) is an effective means of preventing stroke in patients with symptomatic severe carotid stenosis.[1,2] There is some evidence,[3] though less compelling,[4] that CEA is also effective in patients with asymptomatic stenosis. However, beneficial effects are offset by a small risk of perioperative stroke and death.[5] Perioperative stroke and death rates higher than experienced in published CEA trials jeopardize the efficacy of the procedure, particularly in asymptomatic stenosis.

Thrombo-embolism accounts for 38%[6] to 68%[7] of perioperative neurological events. Most perioperative strokes occur intraoperatively or in the recovery room. During carotid dissection, atheromatous debris may break free and embolise intracranially. Postoperatively, the denuded arterial wall stimulates platelet adhesion, activation, and aggregation leading to thrombosis, embolism, and carotid occlusion.

Transcranial Doppler (TCD) is ideally suited to detect intracranial emboli, which are detected in the Doppler spectrum as high-intensity transient signals. Several investigators have shown an association between embolic signals (ESs) recorded from the ipsilateral middle cerebral artery and development of clinical, radiological, and neuropsychological evidence of ischemia.[8–11]

Our group previously performed a systematic study of ES detection in the high stroke risk early postoperative period.[12] We found 7 of 65 (11%) patients had >50 ES per hour in the early postoperative period, and 5 of these patients had early ischemic neurological symptoms. This led to the hypothesis that detection of frequent postoperative ESs could provide a marker of incipient carotid thrombosis and cerebral ischemia. Further, detection of ESs by TCD could serve as a means of evaluating antithrombotic therapy.

Dextran is a polysaccharide compound commonly used as a volume expander and with known antiplatelet and rheologic properties.[13,14] Dextran reduces platelet adhesion to vascular grafts[15] and improves the patency of lower limb arterial bypass grafts.[16] Lennard and colleagues[17] conducted an open, nonrandomized study in which 5 patients with frequent early postoperative microembolism were given dextran 40, with a reduction in rates of microembolism. Although many vascular surgeons use dextran in the belief that it reduces perioperative stroke, no prospective, randomized, controlled trials have been performed.

We therefore designed a double blind, placebo-controlled, randomized trial to test the efficacy of dextran in this setting. The study involved two phases: Phase 1, to test whether dextran reduces ES in the early postoperative period; and Phase 2, to test whether dextran reduces the incidence of perioperative stroke. Phase 1 has been completed and is the subject of this article.

Patients and Methods

Patients

Sequential patients with carotid artery stenosis undergoing CEA at a major Melbourne University teaching hospital (Austin and Repatriation Medical Center) and its associated private hospital (Warringal Private Hospital) participated in this study. Ethics committee approval for this project was obtained from both centers. Patients diagnosed with symptomatic or asymptomatic carotid artery stenosis in whom CEA was recommended were included. Informed consent was ob-

From the [1]Department of Neurology, John Hunter Hospital, Newcastle; [2]Department of Epidemiology and Preventative Medicine, Monash University, Melbourne; and [3]National Stroke Research Institute and Departments of Neurology and Vascular Surgery, Austin and Repatriation Medical Center, Melbourne, Australia.

Received Feb 9, 2001, and in revised form Jun 27. Accepted for publication Jun 29, 2001.

Published online Sep 4, 2001; DOI: 10.1002/ana.1233

Address correspondence to Dr Donnan, National Stroke Research Institute, Neurosciences Building, Repatriation Campus, Austin and Repatriation Medical Centre, Heidelberg West, Victoria 3081, Australia. Email: donnan@austin.unimelb.edu.au

tained according to the Declaration of Helsinki. Exclusion criteria included congestive cardiac failure, unstable angina or acute myocardial infarction within 3 months of surgery, serum creatinine >0.20mmol/L; platelet count <100,000/mm^3, administration of dextran or other hemodilution therapies over the preceding 72 hours, history of sensitivity to dextran, requirement for continuous intravenous heparin therapy over the first 24 postoperative hours, or inadequate ultrasonic temporal bone windows.

Randomization and Trial Therapy

Computer-generated randomization sequence was administered by the hospital clinical trials pharmacist.

Patients randomized to dextran received an intravenous bolus of 20ml of dextran 1 two minutes before skin incision, to avoid anaphylaxis. This was followed by an intravenous infusion of 1,000ml of 10% dextran 40 in normal saline commenced at the time of skin incision. The first 500ml was administered over 4 hours (125ml/hr) and the second 500ml over the next 12 hours (42ml/hr). Patients randomized to placebo received normal saline instead of dextran using equivalent volumes and rates of infusion.

Concomitant Antithrombotic Medication

Most patients were on antiplatelet drugs throughout the perioperative period. In some patients, at the surgeon's discretion, antiplatelet therapy was ceased 24 hours before surgery and recommenced 24 to 48 hours after surgery. Anticoagulants were ceased preoperatively. All patients received an intraoperative bolus dose of heparin, reversed with protamine at the surgeon's discretion following arteriotomy closure.

Transcranial Doppler Monitoring

A 2MHz, portable TCD device (DWL, Sipplingen, Germany) was used to insonate the ipsilateral middle cerebral artery through the temporal bone. The monitoring probe was secured by a headband. Monitoring was performed for 30 minutes at 0 to 1 hour, 2 to 3 hours, 4 to 6 hours, and 24 to 36 hours postoperatively. Doppler signals were recorded on digital audiotape for off-line analysis.

Embolic Signal Analysis

Digital audiotapes were reviewed off-line for ES by trained observers blind to clinical details and treatment allocation. A 6dB intensity threshold was used to ensure acceptable accuracy.[18]

Statistical Analysis

Statistical analyses were performed using the *SPSS* for Windows *v 9.0.1* (SPSS, Chicago, IL). To compare the number of ESs between treatment groups, the nonparametric Wilcoxon Mann-Whitney *U* test was used. The a priori hypothesis was that dextran reduces ES counts in the 0- to 1-hour postoperative epoch.

Results

Of a potential pool of 302 patients undergoing CEA, 150 were randomly assigned. Most of the remainder was not randomly assigned for logistical reasons. Of the 150 patients randomly assigned, 2 patients did not have CEA, another withdrew from the study, 3 did not have TCD recordings, 2 did not have a technically satisfactory recording, and 1 tape was lost. There were therefore 141 patients (69 placebo group, 72 dextran group) with analyzable TCD records in the 0- to 1-hour epoch. The 2 groups were well balanced, with no significant differences between baseline characteristics (Table 1). There were 117 recordings available for the 2- to 3-hour epoch, 116 for the 4- to 6-hour epoch, and 102 for the 24- to 36-hour epoch. Reasons for failure to obtain later recordings included after-hours logistics, clinical deterioration, and commencement of open-label dextran or anticoagulant therapy.

During the 0- to 1-hour postoperative period, ESs were recorded from 39 of 69 (57%) patients who received placebo and 30 of 72 (42%) receiving dextran (Table 2). Total ES counts were 46% lower in the dextran group (Fig) ($p = 0.052$, Wilcoxon-Mann-Whitney *U* test).

During the 2- to 3-hour postoperative period, ESs were recorded from 26 of 58 (45%) patients who received placebo and 16 of 59 (27%) patients who received dextran (see Table 2). Total ES counts were 64% lower in the dextran group ($p = 0.040$).

During the 4- to 6-hour postoperative period, total ES counts were 91% lower in the dextran group (see Table 2). Because these counts were in fewer patients, and the overall number of emboli was lower, only a trend toward a beneficial effect was seen ($p = 0.13$). There was no discernable difference between the 2 groups at 24 to 36 hours after CEA ($p = 0.84$).

Antiplatelet therapy (mostly aspirin) was administered to 76% of the dextran group and 84% of the placebo group in the 7 days prior to surgery. Post hoc analysis of 0- to 1-hour data revealed a probable anti-

Table 1. Baseline Characteristics of 141 Patients with Postoperative Embolic Signal Analysis Assigned to Receive Dextran or Placebo

Characteristic	Treatment Group	
	Dextran (n = 72)	Placebo (n = 69)
Mean age (yr) ± SD	69.0 ± 7.6	69.5 ± 8.7
Male gender	69%	75%
Hypertension	67%	70%
Diabetes	11%	15%
Ischemic heart disease	39%	46%
Peripheral vascular disease	33%	39%
Smoking (current)	18%	12%
Smoking (past)	58%	64%
Antiplatelet therapy within 7 days of surgery	76%	84%
Intraoperative reversal of heparin by protamine	68%	67%

Table 2. Comparison of Embolic Signal Counts in Placebo and Dextran Treatment Groups According to Time After Carotid Endarterectomy

	Placebo				Dextran				
Time Postop (hr)	ES + ve	Total ES	ES/30 min	Mean Rank[a]	ES+	Total ES	ES/30 min	Mean Rank[a]	p^a
0–1 (n = 141)	39/69 (57%)	656	0–118	77.4	30/72 (42%)	354	0–78	64.9	0.052
2–3 (n = 117)	26/58 (45%)	387	0–123	64.6	16/59 (27%)	138	0–88	53.5	0.040
4–6 (n = 116)	17/58 (29%)	273	0–105	62.1	12/58 (21%)	25	0–13	54.9	0.130
24–36 (n = 102)	11/49 (22%)	86	0–33	51.1	13/53 (25%)	85	0–35	51.9	0.840

[a]Wilcoxon Mann-Whitney *U* test.

ES + ve = patients in whom embolic signals are detected.

platelet effect on ES counts and possible interaction between dextran and antiplatelet therapy. Median ES counts were: neither drug, 6; dextran alone, 2; antiplatelet alone, 1; and both drugs, 0. Furthermore, using stepwise logistical regression analysis for treatment with dextran, antiplatelet therapy and dextran × antiplatelet interaction, with presence or absence of emboli as the dependent variable, dextran was rejected from the model whereas antiplatelet therapy ($p = 0.0011$) and dextran × antiplatelet interaction ($p = 0.0390$) were included. However, this does not take into consideration any decrease in high numbers of emboli. Intraoperative reversal of heparin by protamine had no effect on ES counts.

No allergic reactions occurred in either dextran or placebo groups. Eleven patients (7 dextran group, 4 placebo group, not significant) developed wound hematoma, of whom 7 were returned to the operating room for surgical evacuation and hemostasis. Other surgical complications were not overrepresented in the dextran group.

Discussion

In patients undergoing CEA, intravenous infusion of 10% dextran 40 beginning from the time of skin incision produced a reduction in ESs in the early postoperative period, corresponding to a period of high stroke risk.[6,7] Our results are consistent with the mechanism for postoperative strokes being platelet adhesion, activation, and aggregation, which culminate in embolism or carotid occlusion and hemodynamic insufficiency.

This study is novel in a number of ways. It is the first large randomized, double blind, placebo-controlled trial to use ESs as an endpoint in the evaluation of an antithrombotic drug. It is also the first randomized, controlled trial to examine the antithrombotic effect of 10% dextran 40 in the early postoperative period of CEA. In a smaller trial involving 24 patients undergoing CEA, Molloy and colleagues[19] showed that S-nitrosoglutathione, a nitric oxide donor with relative platelet specificity, also reduced ESs.

Although a reduction in ESs from treatment with

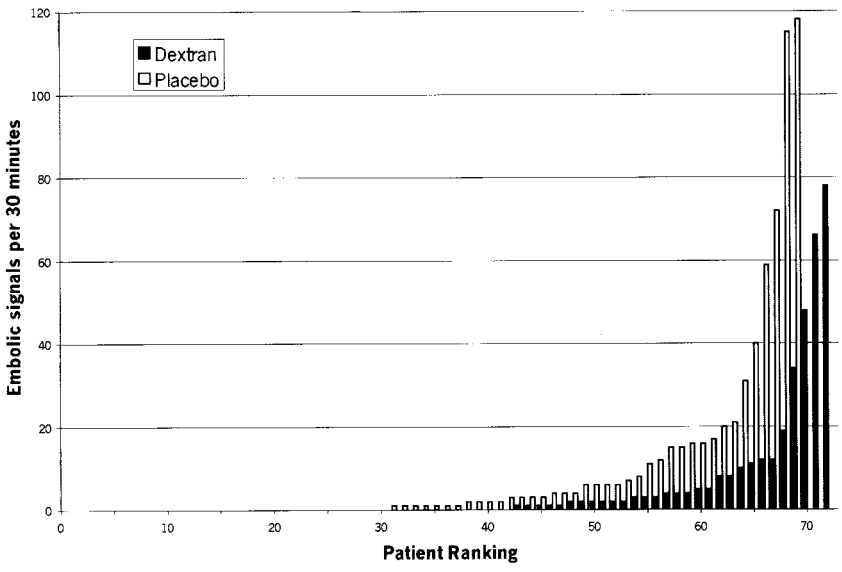

Fig. Emboli counts per 30-minute recording during the 0- to 1-hour postoperative period in individual patients in dextran and placebo groups, ranked within each group according to increasing emboli counts.

dextran may reduce the rate of postendarterectomy stroke, this remains to be established. Hence, we continue to randomize patients into Phase 2 of the study, to determine clinical outcome.

TCD is safe, noninvasive, relatively simple, and inexpensive. If Phase 2 demonstrates that dextran reduces postoperative stroke, then TCD emboli counts may be a useful surrogate for clinical outcome in future trials of antithrombotic agents in the setting of CEA, thereby reducing sample size requirements substantially.

We thank Dr John Ludbrook for his helpful review of the statistical analysis.

References

1. North American Symptomatic Carotid Endarterectomy Trial Collaborators. Benefit of carotid endarterectomy in patients with symptomatic moderate or severe stenosis (NASCET). N Engl J Med 1998;339:1415–1425.
2. European Carotid Surgery Trialists' Collaborative Group (ECST). Randomised trial of endarterectomy for recently symptomatic carotid stenosis: final results of the MRC European Carotid Surgery Trial (ECST). Lancet 1998;351:1379–1387.
3. Executive Committee for the Asymptomatic Carotid Atherosclerosis Study (ACAS). Endarterectomy for asymptomatic carotid artery stenosis. JAMA 1995;273:1421–1428.
4. Chambers BR, You RX, Donnan GA. Carotid endarterectomy for asymptomatic carotid stenosis (Cochrane Review). The Cochrane library (issue 1). Oxford: Update Software, 2001.
5. Rothwell PM, Warlow CP. Is self-audit reliable? Lancet 1995; 346:1623.
6. Riles TS, Imparato AM, Jacobowitz GR, et al. The cause of perioperative stroke after carotid endarterectomy. J Vasc Surg 1994;19:206–216.
7. Krul JMJ, van Gijn J, Ackerstaff RGA, et al. Site and pathogenesis of infarcts associated with carotid endarterectomy. Stroke 1989;20:324–328.
8. Spencer MP, Thomas GI, Nicholls SC, Sauvage LR. Detection of middle cerebral artery emboli during carotid endarterectomy using transcranial Doppler ultrasonography. Stroke 1990;21: 415–423.
9. Jansen C, Ramos LMP, van Heesewijk JPM, et al. Impact of microembolism and hemodynamic changes in the brain during carotid endarterectomy. Stroke 1994;25:992–997.
10. Gaunt ME, Martin PJ, Smith JL, Rimmer T, et al. Clinical relevance of intraoperative embolization detected by transcranial Doppler ultrasonography during carotid endarterectomy: a prospective study of 100 patients. Br J Surg 1994;81:1435–1439.
11. Levi CR, Bladin CF, Chambers BR, et al. Microembolic watershed infarction complicating carotid endarterectomy. Cerebrovasc Dis 1997;7:185–186.
12. Levi CR, O'Malley HM, Fell G, et al. Transcranial Doppler detected cerebral microembolism following carotid endarterectomy: high microembolic signal loads predict post-operative cerebral ischaemia. Brain 1997;120:621–629.
13. Weiss HJ. The effect of clinical dextran on platelet aggregation, adhesion and ADP release in man: in vivo and in vitro studies. J Lab Clin Med 1967;69:37–46.
14. Ljungstrom KG. The antithrombotic efficacy of dextran. Acta Chir Scand 1988;543(suppl):26–30.
15. Christenson JT, Al-Huneidi W, Saleh RA. Distal embolisation from the surface of PTFE grafts in vivo and the effects of low molecular weight dextran. Eur J Vasc Surg 1988;2:121–125.
16. Rutherford RB, Jones DN, Bergentz SE, et al. The efficacy of dextran 40 in preventing post-operative thrombosis following difficult lower extremity bypass. J Vasc Surg 1984;1:765–773.
17. Lennard N, Smith J, Dumville J, et al. Prevention of postoperative thrombotic stroke after carotid endarterectomy: the role of transcranial Doppler ultrasound. J Vasc Surg 1997;26: 579–584.
18. Markus HS, Ackerstaff R, Babikian V, et al. Intercenter agreement in reading Doppler embolic signals. A multicenter international study. Stroke 1997;28:1307–1310.
19. Molloy J, Martin JF, Baskerville PA, et al. S-Nitrosoglutathione reduces the rate of embolization in humans. Circulation 1998; 98:1372–1375.

Mutation of the Doublecortin Gene in Male Patients with Double Cortex Syndrome: Somatic Mosaicism Detected by Hair Root Analysis

Mitsuhiro Kato, MD,[1] Masayo Kanai, MD,[1] Osamu Soma, MD,[2] Yuichi Takusa, MD,[3] Toshiyuki Kimura, MD,[1] Chikahiko Numakura, MD,[1] Takasumi Matsuki, MD,[4] Shigeki Nakamura, PhD,[5] and Kiyoshi Hayasaka, MD[1]

The molecular basis of double cortex syndrome was investigated in 2 male patients. Magnetic resonance imaging of the patients' heads showed diffuse subcortical band heterotopia, as is seen in female patients. We found a heterozygous mutation for Asp50Lys or Arg39Stop in both patients. Microsatellite polymorphism analysis revealed that both patients had inherited a single X chromosome from their mothers. Restriction enzyme analysis

From the [1]Department of Pediatrics, Yamagata University School of Medicine, Yamagata; [2]Department of Development and Neurology, Kobe Children's Hospital, Kobe; [3]Department of Pediatrics, Shimane Medical University, Izumo, Shimane; [4]Department of Forensic Medicine, Fukui Medical University, Fukui; and [5]Department of Legal Medicine, Kitasato University School of Medicine, Sagamihara, Kanagawa, Japan.

Received Feb 19, 2001, and in revised form Jul 9. Accepted for publication Jul 9, 2001.

Published online Sep 3, 2001; DOI: 10.1002/ana.1231

Address correspondence to Dr Kato, Department of Pediatrics, Yamagata University School of Medicine, Iida-nishi 2-2-2, Yamagata 990-9585, Japan. E-mail: mkato@med.id.yamagata-u.ac.jp

using DNA extracted from the hair roots of each patient showed four different patterns in the combination of cells carrying wild and mutant alleles, which strongly suggest somatic mosaicism. We conclude that somatic mosaic mutations in the doublecortin gene in male patients can cause subcortical band heterotopia, and that molecular analysis using hair roots is a useful method for detecting somatic mosaicism.

Ann Neurol 2001;50:547–551

X-linked lissencephaly and subcortical band heterotopia,[1] or double cortex syndrome,[2] is a brain malformation involving diffuse cortical dysplasia, and is characterized on magnetic resonance images (MRIs) as bilateral continuous symmetric bands of gray matter underlying the cortical mantle (subcortical band heterotopia [SBH]) in female patients. The major clinical manifestations are epilepsy and mild to moderate mental retardation. Affected sons of a mother with SBH show classic lissencephaly (smooth brain), a more severe form of cortical dysplasia. Linkage analysis and subsequent positional cloning have led to the isolation of a novel gene, doublecortin (*DCX*), mapping to Xq22.3–Xq23.[3,4] It has been revealed that females with heterozygous *DCX* mutations develop band heterotopia, and males with *DCX* hemizygous mutations develop classic lissencephaly.[5] On the other hand, a relatively small number of male patients with band heterotopia has been reported.[6] Although the results of one study based on single-stranded conformational polymorphism analysis and direct sequencing has suggested somatic mosaicisms for the *DCX* mutation,[7] another study has demonstrated missense mutations of *DCX* or *LIS1*, but failed to provide evidence of somatic mosaicism in male patients with band heterotopia.[8] The mechanism causing a less severe form in male patients is still unclear.

Here, we report on 2 sporadic male patients with SBH in whom molecular analyses of hair roots revealed somatic mosaic mutations in the DCX gene, and in whom microsatellite polymorphisms were located on the X chromosome.

Patients and Methods

Patient 1

Patient 1 was the first child of unrelated healthy parents. He was born at term in a normal delivery after an uncomplicated pregnancy. His body stature was normal at birth. He showed nystagmus from 2 months of age. At 8 years of age, he had recurrent episodes of loss of consciousness and loss of face color. Electroencephalograms (EEGs) revealed focal spike-and-slow-wave discharges in the right occipital area. His seizures were refractory. At 11 years of age, his full scale IQ was 44 (WISC-R). At 12 years of age, MRI revealed SBH, indicating double cortex syndrome (Fig 1A). Results of neurological examination were normal, except for moderate mental retardation. There were no abnormal laboratory findings in biochemical analysis, including liver and renal functions and serum electrolytes. Results of chromosomal analysis were 46XY. EEGs revealed no paroxysmal activity.

Patient 2

Patient 2 was the second child of unrelated healthy parents, whose elder brother showed normal development. Patient 2 was born at term in a normal delivery after an uncomplicated pregnancy. Instability of head control and internal strabismus were noticed at 4 months of age. At 5 months of age, his eyes began to fix and pursuit, but neurological examination demonstrated poor head control. His total developmental quotient was 70 (Japanese Enjoji developmental test). MRI revealed SBH (see Fig 1B). Results of chromosomal analysis were 46XY. EEGs revealed no paroxysmal activity.

Genomic DNA Extraction

After obtaining informed consent from the parents, peripheral blood was taken from the patients and their parents, and

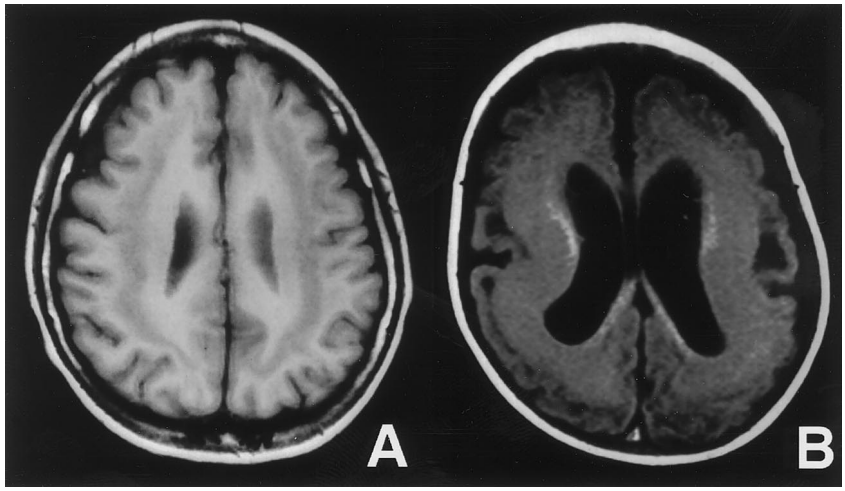

Fig 1. T1-weighted brain magnetic resonance images of Patient 1(A) and Patient 2 (B). Bilateral symmetrical heterotopic gray matter surrounded the periventricular white matter on all sides except the medial region. Sulci are shallow, but not lissencephalic. Patient 2 is more severely affected than Patient 1. Patient 2 showed a reduced volume of cerebral white matter, delayed myelination, and dilatation of the perivascular space.

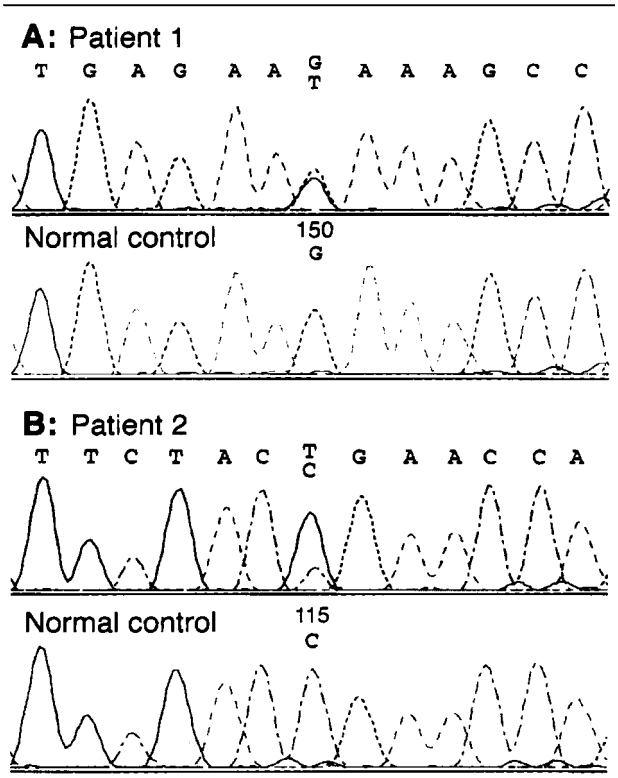

Fig 2. DCX *mutations in Japanese patients with subcortical laminar heterotopia. Direct DNA sequencing of polymerase chain reaction (PCR) products from the patients. (A) The sequence is from nucleotides 144 to 156 of* DCX*, demonstrating a heterozygous G-to-T transition at nucleotide 150 in Patient 1, compared with that in a normal control. (B) The nucleotide sequence of* DCX *in Patient 2 showed a heterozygous C-to-T transversion at nucleotide 115, compared with that in a normal control.*

hair roots were taken from the patients. Genomic DNA from peripheral blood leukocytes and hair roots was extracted using a DNA extraction kit (Nucleon BACC3 for blood and cell cultures, Amersham, Buckinghamshire, UK) according to the manufacturer's instructions, and according to a previous report.[9]

DNA Sequencing

All coding regions of the DCX gene were sequenced using genomic DNA from the patients' peripheral leukocytes. Polymerase chain reaction (PCR) products were amplified as described previously,[10] and sequence analysis was performed on an automated DNA sequencer (ABI 310; Applied Biosystems, Foster City, CA).

Restriction Enzyme Analysis Using Genomic DNA from Hair Roots

A DNA fragment (exon 2.1) was amplified from the genomic DNA of Patient 1, and another DNA fragment (exon 2.2n) was amplified from the genomic DNA of Patient 2 using a set of primers, 2.2F/2.2R, followed by nested PCR with a set of mismatch primers, 2.2F/n2.2R (5′GCCTGCAAGGTTCTGGTGC-3′).[10] Amplified DNA fragments were digested with the restriction enzyme *Mbo*II in Patient 1 and with *Aci*I in Patient 2. They were electrophoresed on a 3% agarose gel and a 15% polyacrylamide gel, respectively.

Evaluation of Parental Origin Analyzed by Microsatellite Polymorphisms

Genomic DNA from the peripheral leukocytes of the patients and their parents were analyzed using short tandem repeat systems located on the full length of the X chromosome.[11] PCR amplification was performed with an ABI PRISM Linkage Mapping Set-MD 10 Panel 28 (Applied Biosystems) according to the manufacturer's instructions. Control DNA CEPH 1347-02 was used as a reference for allele designation using *Gene Scan Analysis v 2.1* software.

Results

DNA sequence analysis of coding regions (exons 2–6) showed that Patient 1 had a G-to-T substitution at nucleotide number 150, which resulted in an asparagine substitution for lysine at codon 50 (Fig 2A). Patient 2 demonstrated a C-to-T transition at nucleotide number 115, which resulted in an arginine–to–stop codon substitution at codon 39 (see Fig 2B). The patients were heterozygous for mutant and wild alleles. Their parents did not carry these mutations, suggesting that the mutations were de novo.

Restriction enzyme analysis of the products from the hair roots of each patient showed four patterns (Fig 3). They represented the product from only the wild allele, the mixed product from a more-wild allele and a less-mutant allele, the mixed product from a less-wild allele and a more-mutant allele, and the product from only a mutant allele. The mutant allele was segregated from the wild allele, suggesting somatic mosaicism.

Microsatellite polymorphism analysis showed that each patient had a single allele of each marker on the X chromosome of the mother (data not shown), indicating that each patient had inherited a single X chromosome from his mother. These results indicated that the patients represented a somatic mosaic mutation, but not a chimera, and suggested that the mutation of the DCX gene located on an X chromosome inherited from the mother occurred during early embryogenesis.

Discussion

We analyzed mutations in the DCX gene in 2 male patients with SBH, and identified two novel heterozygous mutations. Because the patients showed normal karyotypes, it was thought that they were mosaics or chimeras. Microsatellite analysis showed that each patient had inherited a single allele of each marker located on the X chromosome of his mother. These results indicate that neither of the patients are chimeras. Hair roots have been used as material to confirm somatic mosaicism.[12] We therefore performed PCR and restriction enzyme analysis using DNA extracted from

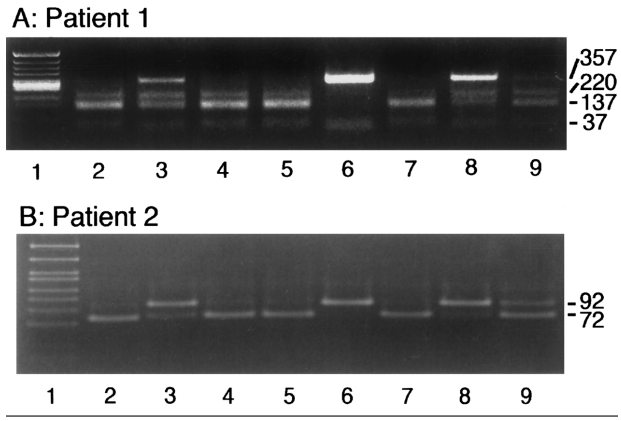

*Fig 3. Electrophoresis of the Mbo*II *(A, Patient 1) or Aci*I *(B, Patient 2) digestion fragment of PCR products of exon 2.1 (A) or exon 2.2n (B). Lane* 1*, size marker digest (A, fX174/Hinc II; B, fX174/Hinf I). Lane* 2*, normal control. Lane* 3*, blood sample from the patient. Lane* 4*, patient's father. Lane* 5*, patient's mother. Lanes* 6–9*, hair roots from the patient. (A) The PCR product (394 bp fragment) is normally cleaved by the endonuclease Mbo*II *into three fragments of 220, 137, and 37 bp (lanes* 2, 4, *and* 5*). The 37 bp fragment in A is faint. The mutant allele deleted a Mbo*II *site, producing a 357-bp band and a 37 bp band. A sample obtained from the patient's blood showed both a 357 bp band and a shorter band, indicating heterozygosity. (B) The PCR product (92 bp fragment) is normally cleaved by the endonuclease Aci*I *into two fragments of 72 and 20 bp (lanes* 2, 4, *and* 5*). The 20 bp fragment could not be visualized on this gel. The mutant allele deleted an Aci*I *site, producing only a 92 bp band. A sample obtained from the patient's blood showed both 92 bp and 72 bp bands, indicating heterozygosity. Electrophoresis of hair roots from both patients demonstrated four different patterns: a mutated homozygous pattern (lane* 6*); a normal homozygous pattern (lane* 7*); an abnormal heterozygous pattern, which showed a thicker mutant band than the normal band (lane* 8*); and an abnormal heterozygous pattern, in which the normal band is thicker than mutant band (lane* 9*).*

hair roots. Recently, multipotent stem cells that generate all the lineages of the hairy skin in adult mice were found.[13] Because three progenitor cells are commonly involved in the development of one human hair root,[14] a male patient with somatic mosaicism of the DCX gene is expected to have four types of hair roots, consisting of cells carrying only the wild allele; mixed cells carrying the wild or mutant allele (ratio of 2:1); mixed cells carrying the wild or mutant allele (ratio of 1:2); and cells carrying only the mutant allele. The results of hair root analysis coincided with the above hypothesis, and proved that the patients had somatic mosaicisms. Lymphocytes (mesodermal derivatives) and hair roots (ectodermal derivatives) showed mosaicism; therefore, their somatic *DCX* mutations showed generalized mosaicism. These results suggest that the mutation of the DCX gene may have occurred during early postzygotic division.[15]

There are conflicting reports as to whether *DCX* mutations in males with double cortex syndrome indicate mosaicism.[7,8] Because mosaicism can vary between tissues, molecular analysis using lymphocytes may not show mutation. On the other hand, hair roots as well as brain are ectodermal derivatives. Hair root analysis would therefore be better than blood analysis for establishing somatic mosaicism of the brain. In addition, there are some SBH patients without *DCX* mutations in DNA extracted from peripheral lymphocytes, particularly patients with posterior dominant or focal heterotopia.[10,16,17] Hair root analysis may also be advantageous for detecting somatic mosaicism localized in one part of the brain.

Factors influencing the severity of brain malformations include mutational genes, location and type (such as missense or nonsense) of the mutation,[5,17] distribution of mutation (X chromosome inactivation or somatic mosaicisms), and other modifying agents (such as environment and other genes). Gleeson and colleagues analyzed the ratio of mosaicism using quantitative PCR reaction or densitometry of single-stranded conformational polymorphism bands,[7] and they suggested that individuals with a higher mutation load are likely to be more severely affected. In our study, Patient 2 showed more severe brain malformation, diffusely thick-band heterotopia, and hypoplastic gyral formation than did Patient 1. We did not estimate the ratio of mosaicism, but the results of restriction analysis using genomic DNA isolated from peripheral leukocytes suggested that there was a larger number of cells carrying mutation alleles in Patient 2 (see Fig 3B, lane 3) than in Patient 1. In addition, it was thought that the nonsense mutation at exon 2 of Patient 2 would have produced a truncated protein that may be toxic and may be related to the severity in Patient 2. Further cases should be analyzed to make clear genotype-phenotype relationships.

This study was supported in part by the Ministry of Education, Science and Culture and from the Epilepsy Research Foundation, Japan.

We thank Dr Toshio Ohsima and Professor Katsuhiko Mikoshiba, Developmental Neuroscience Group, Brain Science Institute, RIKEN, for their helpful suggestions.

References

1. Dobyns WB, Truwit CL. Lissencephaly and other malformations of cortical development: 1995 update. Neuropediatrics 1995;26:132–147.
2. Palmini A, Andermann F, Aicardi J, et al. Diffuse cortical dysplasia, or the 'double cortex' syndrome: the clinical and epileptic spectrum in 10 patients. Neurology 1991;41:1656–1662.

3. Gleeson JG, Allen KM, Fox JW, et al. Doublecortin, a brain-specific gene mutated in human X-linked lissencephaly and double cortex syndrome, encodes a putative signaling protein. Cell 1998;92:63–72.
4. des Portes V, Pinard JM, Billuart P, et al. A novel CNS gene required for neuronal migration and involved in X-linked subcortical laminar heterotopia and lissencephaly syndrome. Cell 1998;92:51–61.
5. Gleeson JG, Minnerath SR, Fox JW, et al. Characterization of mutations in the gene doublecortin in patients with double cortex syndrome. Ann Neurol 1999;45:146–153.
6. Ono J, Mano T, Andermann E, et al. Band heterotopia or double cortex in a male: bridging structures suggest abnormality of the radial glial guide system. Neurology 1997;48:1701–1703.
7. Gleeson JG, Minnerath S, Kuzniecky RI, et al. Somatic and germline mosaic mutations in the *doublecortin* gene are associated with variable phenotypes. Am J Hum Genet 2000;67: 574–581.
8. Pilz DT, Kuc J, Matsumoto N, et al. Subcortical band heterotopia in rare affected males can be caused by missense mutations in *DCX* (*XLIS*) or *LIS1*. Hum Mol Genet 1999;8: 1757–1760.
9. Higuchi R, von Beroldingen CH, Sensabaugh GF, Erlich HA. DNA typing from single hairs. Nature 1988;332:543–546.
10. Kato M, Kimura T, Lin C, et al. A novel mutation of the doublecortin gene in Japanese patients with X-linked lissencephaly and subcortical band heterotopia. Hum Genet 1999; 104:341–344.
11. Sawazaki K, Tsubota E, Iida R, Matsuki T. DXS10011 typing by capillary electrophoresis. Jpn J Leg Med 2000;54:467.
12. Putnam EA, Park ES, Aalfs CM, et al. Parental somatic and germ-line mosaicism for a FBN2 mutation and analysis of FBN2 transcript levels in dermal fibroblasts. Am J Hum Genet 1997;60:818–827.
13. Oshima H, Rochat A, Dedzia C, et al. Morphogenesis and renewal of hair follicles from adult multipotent stem cells. Cell 2001;104:233–245.
14. Dancis J, Silvers DN, Balis ME, et al. Evidence for the derivation of individual hair roots from three progenitor cells. Hum Genet 1981;58:414–416.
15. Kalousek DK. Pathogenesis of chromosomal mosaicism and its effect on early human development. Am J Med Genet 2000; 91:39–45.
16. Gleeson JG, Luo RF, Grant PE, et al. Genetic and neuroradiological heterogeneity of double cortex syndrome. Ann Neurol 2000;47:265–269.
17. Matsumoto N, Leventer RJ, Kuc JA, et al. Mutation analysis of the DCX gene and genotype/phenotype correlation in subcortical band heterotopia. Eur J Hum Genet 2001;9:5–12.